

Review

# Metal–Organic Frameworks as Powerful Heterogeneous Catalysts in Advanced Oxidation Processes for Wastewater Treatment

Antía Fdez-Sanromán, Emilio Rosales , Marta Pazos  and Angeles Sanroman \* 

CINTECX, Department of Chemical Engineering, Universidade de Vigo, Campus Universitario As Lagoas—Marcosende, 36310 Vigo, Spain

\* Correspondence: sanroman@uvigo.es

**Abstract:** Nowadays, the contamination of wastewater by organic persistent pollutants is a reality. These pollutants are difficult to remove from wastewater with conventional techniques; hence, it is necessary to go on the hunt for new, innovative and environmentally sustainable ones. In this context, advanced oxidation processes have attracted great attention and have developed rapidly in recent years as promising technologies. The cornerstone of advanced oxidation processes is the selection of heterogeneous catalysts. In this sense, the possibility of using metal–organic frameworks as catalysts has been opened up given their countless physical–chemical characteristics, which can overcome several disadvantages of traditional catalysts. Thus, this review provides a brief review of recent progress in the research and practical application of metal–organic frameworks to advanced oxidation processes, with a special emphasis on the potential of Fe-based metal–organic frameworks to reduce the pollutants present in wastewater or to render them harmless. To do that, the work starts with a brief overview of the different types and pathways of synthesis. Moreover, the mechanisms of the generation of radicals, as well as their action on the organic pollutants and stability, are analysed. Finally, the challenges of this technology to open up new avenues of wastewater treatment in the future are sketched out.

**Keywords:** electro-Fenton; Fenton; heterogeneous catalyst; MOFs; pharmaceutical and personal care products; photocatalyst; ozone



**Citation:** Fdez-Sanromán, A.; Rosales, E.; Pazos, M.; Sanroman, A. Metal–Organic Frameworks as Powerful Heterogeneous Catalysts in Advanced Oxidation Processes for Wastewater Treatment. *Appl. Sci.* **2022**, *12*, 8240. <https://doi.org/10.3390/app12168240>

Academic Editor: Leonarda Francesca Liotta

Received: 28 July 2022

Accepted: 15 August 2022

Published: 17 August 2022

**Publisher's Note:** MDPI stays neutral with regard to jurisdictional claims in published maps and institutional affiliations.



**Copyright:** © 2022 by the authors. Licensee MDPI, Basel, Switzerland. This article is an open access article distributed under the terms and conditions of the Creative Commons Attribution (CC BY) license (<https://creativecommons.org/licenses/by/4.0/>).

## 1. Introduction

The demographic growth in developed countries and consequently, the demand for products from agriculture, livestock and industry has increased and led to a significant development of the related industries [1]. However, despite the magnificent benefits provided to society, there is evidence that soil, water and atmosphere are still being polluted [2]. Among these major environmental problems, the water environment is of particular importance because it is a valuable and limited resource [3]. Further, the wastewater treatment plants (WWTP) of today are not capable of degrading or removing persistent organic pollutants from wastewater. These organic pollutants, including the newly recognized emerging persistent organic pollutants, have increasingly been detected in recent years [4]. This term typically refers to substances that have been introduced to the environment or that have been discovered in nature, whether they are synthetic or natural. Persistent organic pollutants are generated from compounds applied for a range of purposes including pharmaceuticals and personal care products, pesticides, food additives and dyes from the textile industry [4]. Therefore, as this problem instead of diminishing has had the opposite effect, efforts to develop new and more efficient and environmentally sustainable technologies are urgently needed.

Of all the recent technologies developed up-to-date, Advanced Oxidation Processes (AOPs) are the most efficient in removing these persistent organic pollutants from aqueous media and are considered eco-friendly treatment processes. These helpful processes are

based on the in situ production of non-selective radicals with a strong oxidation power able to mineralize the organic pollutants. Among the mentioned radicals, hydroxyl ( $\text{HO}^\bullet$ ), sulphate ( $\text{SO}_4^{\bullet-}$ ) and superoxide ( $\text{O}_2^{\bullet-}$ ) radicals are the most used since they give the highest oxidative capacity and have better environmental properties [5]. Producing these radicals is a complex process that requires a catalyst for their generation by different activation methods. Moreover, to improve the AOPs, alternative catalysts to the conventional ones are required.

Among the different alternatives, metal–organic frameworks (MOFs) have arisen as suitable options since they are of great interest for their use in wastewater treatment. The first time that a MOF was used as a heterogeneous catalyst in an oxidation process was reported by De Rosa et al. [6]. They developed an efficient heterogeneous catalytic pre-treatment of Olive oil mill wastewaters (OOMW) in which the biodegradability of the OOMW was increased to make possible the subsequent biological oxidation. The used MOF contained copper,  $\text{Cu}_3(\text{BTC})_2(\text{H}_2\text{O})_3$  (BTC = benzene 1,3,5-tricarboxylic acid), showing a high micropore volume, large pore sizes, crystallinity, and a high metal content. In comparison to the homogeneous catalyst, this material provided good properties to significantly improve the biodegradability of the OOMW and opened the possibility to recover the catalyst and reuse it. These results clearly revealed the great potentialities of MOFs as a catalyst that have attracted much attention for exploiting new applications of MOFs in wastewater treatment. However, they have the great disadvantage that many of them are not stable in water. Besides this, it is also important to keep in mind that, as with any synthesis, a high level of purity is reached, but they always contain impurities or do not have the desired morphology [7]. Therefore, in recent years, one of the main aims of MOF synthesis has been the development of alternatives to conventional methods to improve production yields and control their morphology [7].

The main goal of this work is to highlight recent progress in applying MOF derivatives as emerging efficient heterogeneous catalysts for the removal of organic persistent pollutants by different AOPs. For the generation of oxidative radicals in AOPs, the activation by transition metals such as ferrous ion, which is a cost-effective and environmentally friendly catalyst, is necessary. In the last few years, iron-based heterogeneous catalysts have replaced these homogeneous catalysts. Among the recent materials, Fe-MOFs with highly ordered structural and porous crystals can be considered a potential alternative to overcome a number of drawbacks associated with traditional water treatment. Thus, the structures can be rationally designed through the facile control of the architecture and functionalization of the pores favouring the removal of selective pollutants. For this reason, this study starts by describing the different types, structures, composition and preparation strategies of MOFs, and then focuses on the more used MOFs in AOPs, FeMOFs derivatives in Fenton, Fenton-like, electro-Fenton, and photo-Fenton, photoelectron-Fenton, and ozone processes, including organic pollutant (especially pharmaceuticals) removal, influencing factors, reusability and stability.

## 2. MOFs

MOFs are known as an innovative class of highly porous and crystalline organic–inorganic hybrid materials made by linking organic molecules with metal ions [8]. An organic skeleton surrounds this metal cluster, providing a stable structure and reducing the release of metal into the medium [9,10]. MOF structures show great diversity and the way the components are organized makes it possible to obtain a certain structure with different properties in the function of the desired purpose [11].

In recent years, they have shown great potential for various engineering applications (adsorption, catalysis, electrochemistry, etc.) [12]. A shedload of accessible active sites and a high specific surface area are also responsible for their increased interest [13,14]. Their ability to be modified and functionalized also allows them to be used in very explicit applications, such as luminous sensors for different analyses [15] to the removal of pharmaceuticals from wastewater [16]. In fact, this last application is highlighted because in the

last five years there has been an increase in their use in wastewater treatment by means of AOPs. Despite advances in science, MOFs still struggle with many operational issues, including the stability of these materials in aqueous environments or the ability to recover and reuse them under certain conditions [17]. Therefore, the search for new MOFs is a reality. In what follows, brief descriptions of the different types of MOFs used today for wastewater treatment and the most frequent synthesis techniques are given.

### 2.1. Most Useful Types of MOF for Wastewater

As mentioned above, MOFs consist of an inorganic part, usually transition metals (Cr, Mn, Co, Ni, Fe, Cu, Zn, . . . ), as they have a high charge density, and an organic part [18]. Hence, when the ligands and the coordination environment remain the same, the metal ions can form stronger coordination bonds and, consequently, such a MOF will be more stable. This behaviour is due to Pearson's hard/soft acid/base (HSAB) principle [18].

Metal ions and ligands produce different morphologies, depending on their combination. Among the great variety that currently exists (Figure 1), the MIL (Lavoisier Institute Material), the ZIF (Zeolite Imidazolate Framework), the UiO (Universitetet i Oslo) and the HKUST (Hong Kong University of Science and Technology) stand out.

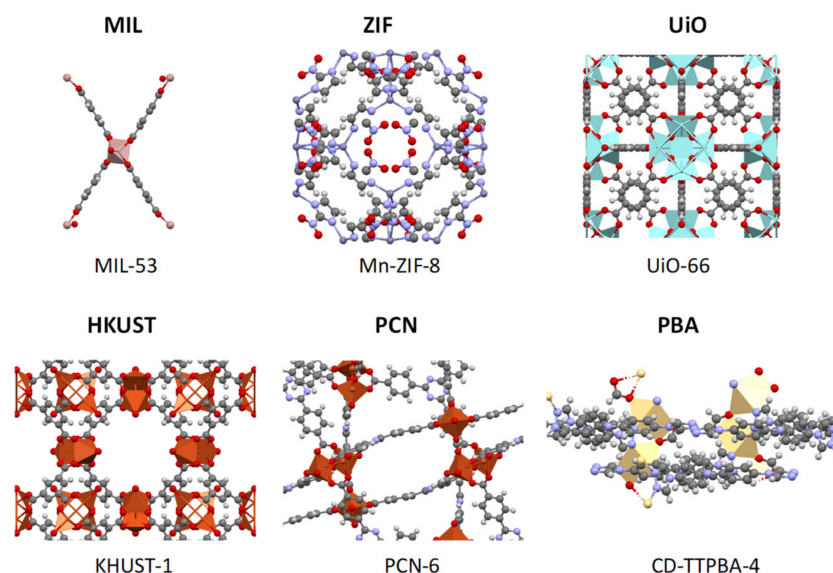


**Figure 1.** MOF structures (reproduced from CSD MOF Collection [19] under license CC BY-NC-SA 4.0).

These MOFs have been widely used in wastewater treatment in recent years, as shown in Figure 2. Figure 2 also includes the PBA (Prussian Blue Analogues) [20] and PCN (Porous Coordination Network) [21,22] because, although the number of current publications is very small, these materials are promising, since several studies have demonstrated that PCN and PBA can be viable alternatives to other MOFs when it comes to removing pollutants from water [23–26].

In Figure 2, the results of the literature search for the range 2018 to 2022 are represented and the keywords used were “metal-organic framework”, “wastewater” and the abbreviation of the given MOFs (MIL, ZIF, . . . ). Clearly, these profiles showed a considerable increase in the number of papers, which demonstrates the progress and feasibility of MOFs in water treatment, mainly when MIL, ZIF and UiO MOFs are used. As for the results for the year 2022, since the year has not yet ended, they could not be fully evaluated. The only conclusion that can be reported is that, even before the end of the year, the number of publications was very similar to 2020, so, with this evolution, it is intuited that the numbers will be higher than in 2021.

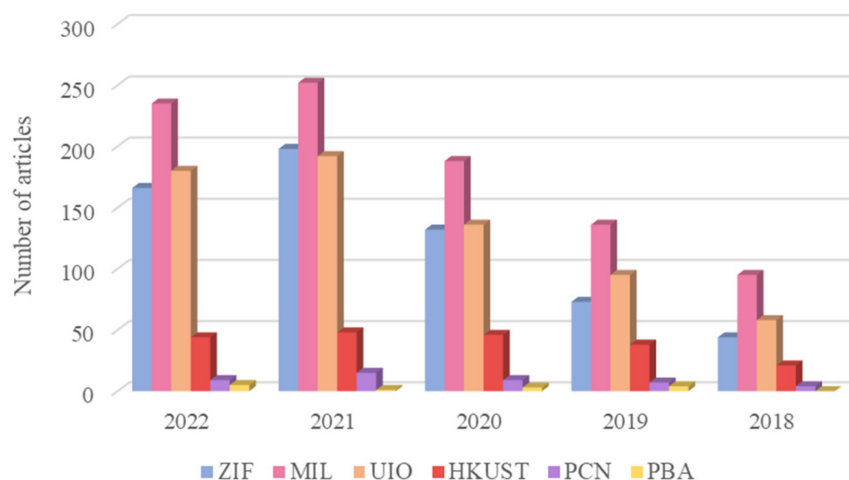


**Figure 2.** Evolution of the number of published articles on wastewater treatment for each type of MOF in the last five years.

### 2.1.1. MIL

These MOFs are characterized by ligands based on carboxylates, which can be considered hard bases according to the HSAB principle. In this case, the MOFs are stable because of the use of metal ions with high valences, such as the cations  $Al^{3+}$ ,  $Ti^{4+}$ ,  $Fe^{3+}$  or  $Cr^{3+}$  [18]. A key characteristic of these catalysts is their flexibility, which allows them to be modified and functionalized in different ways [27]. In order to optimize pollutant removal processes, it is necessary to research functionalized MIL-type MOFs. Table 1 presents some of the MILs used to treat wastewater; it is important to note that Fe-MILs are the most commonly used MOF, followed by Cr, Al and Ti.

**Table 1.** Applications of MIL–MOF in wastewater treatment.

MIL	Pollutant	Processes	Reference
AgCl/MIL-100(Fe)	Sulfamethazine (SMT)	Photocatalytic	[28]
BC@FexC	Norfloxacin	Catalytic activation of peroxydisulfate (PDS)	[29]
NCQDs/MIL-101(Fe)	Tetracycline (TC)	Photo-Fenton and Photocatalytic	[30]
MIL-101(Cr)@AC	Sulfacetamide	Adsorption	[31]
MIL-125(Ti)	TC	Photocatalytic	[32]
MIL-125(Ti)/BiOI	Rhodamine B and TC	Photocatalytic	[33]
MIL-53(Al)@SiO <sub>2</sub>	Bisphenol A	Photocatalytic	[34]
MIL-53(Al)-NDC	Tinidazole	Adsorption	[35]
Mn-MIL-53(Fe)	TC	Catalytic activation of PMS	[36]
(PDI)/MIL-101(Cr)	Iohexol	Photocatalytic activation of PDS	[36]

### 2.1.2. ZIF

The next class of MOFs is the second most commonly used. They are considered topologically isomorphic to zeolites (Figure 1) [37]. Thus, their structures are generated according to tetrahedral units where every metal ion (M) attaches to four organic imidazolate (Im) linkers (M-Im-M) [37,38]. According to the HSAB principle, this structure can be made stable when assembled by soft azolate ligands, such as imidazoles, pyrazoles or triazoles and soft divalent metal ions, in this case, Zn, Co, Cu and Cd [18]. Due to this organisation, they can be characterized by their high surface area, regular pore structure, substantial biocompatibility, scalable synthesis and outstanding thermostability [39]. Moreover, the properties of these materials make them increasingly useful in applications such as gas separation and catalysis [40,41]. In Table 2, some examples demonstrating the use of ZIF in wastewater to remove organic pollutants are shown. The feasibility of its use in this application has been proven due to its upward trend in the number of articles

published from 2018 to 2022 (Figure 2) [42,43]. This type of MOF stands out in adsorption and photocatalysis processes due to the potential that it presents [42].

Many ZIFs have been synthesized to date, but ZIF-8 is among the most widely used since ZIF-8 has the advantage of being synthesized by different routes, regardless of the method selected and can achieve a high purity [44]. However, more environmentally friendly and room temperature syntheses are used nowadays [45].

**Table 2.** Applications of ZIF–MOF in wastewater treatment.

ZIF	Pollutant	Processes	Reference
CZC600-30	TC and methylene blue	Photocatalytic	[46]
MoS <sub>2</sub> @ZNC-2	phenol	Electro-catalytic	[47]
N@ZIF-67	ciprofloxacin	Catalytic activation of PMS	[48]
ZIF-67@WA	TC	Adsorption	[49]
ZIF-9@GEL and ZIF-12@GEL	p-nitrophenol	Catalytic activation of PMS	[50]
ZIF-8	TC and oxytetracycline	Adsorption	[51]
ZnCDs/ZnO@ZIF-8	TC	Photocatalytic	[52]
Zn <sub>2</sub> SnO <sub>4</sub> /SnO <sub>2</sub> @ZIF-8	TC	Photocatalytic	[53]
ZnO/ZIF-9	TC	Photocatalytic	[54]
ZnO@ZIF-67	TC	Adsorption	[55]

### 2.1.3. UiO

UiOs are generally defined as a class of MOFs that are constructed from a zirconium atom and a carboxylic acid as ligands [56]. Specifically, the unit cell consists of an octahedral arrangement formed by a Zr<sub>6</sub>O<sub>4</sub>(OH)<sub>4</sub> cluster that is surrounded by the aforementioned ligands [56]. It should be noted that a structural characteristic of these MOFs is that the cluster is always the same and the only factor that differentiates each type of UiO is the carboxylic acid used as a ligand [57].

The best quality of this type of MOF is that they are the most stable in water even in acidic and basic conditions [58]. In addition to this, they also have properties such as a relatively uniform and large pore size and a specific surface area. The development of modified UiO capable of adsorbing heavy ions is of heightened interest since it is believed to be a reliable and promising solid adsorbent [59]. However, they are also becoming relevant as catalysts for the degradation of pollutants such as dyes or pharmaceuticals [60].

The commonly used UiO classes in scientific works are UiO-66, UiO-67, UiO-68 and UiO-69 [61]. The most widely used among them is UiO-66, either directly or with modifications (Figure 1) [62]. Table 3 below gives some examples of the removal of pharmaceuticals and polycyclic aromatic hydrocarbons from aqueous media. It should be noticed that few works have been found using the MOF type UiO-67, UiO-68 and UiO-69, but its application was only for dye removal [63,64], so they are not included in the table.

**Table 3.** Applications of UiO–MOF in wastewater treatment.

UiO	Pollutant	Processes	Reference
Acid-modulated UiO-66	2,4-dichlorophenoxyacetic acid, ciprofloxacin and naproxen	Adsorption	[62]
C <sub>3</sub> N <sub>4</sub> -TE@TiO <sub>2</sub> /UiO-66	TC	Photocatalytic	[65]
IN <sub>2</sub> S <sub>3</sub> /UiO-66	Methyl orange and TC	Photocatalytic	[66]
MWCNT/N-TiO <sub>2</sub> /UiO-66-NH <sub>2</sub>	Ketoprofen	Photocatalytic	[67]
NiCo <sub>2</sub> O <sub>4</sub> /HP-UiO-66	TC	Photocatalytic with PMS	[68]
UiO-66(Zr) and NH <sub>2</sub> -UiO-66(Zr)	Pyrene	Adsorption	[69]

### 2.1.4. HKUST

Concerning the last type of MOF most commonly used for water treatment, it should be noted that it is based on a copper atom, specifically the copper (II) ion. Only HKUST-1 (Cu-BTC or MOF-199) has been published in scientific articles about HKUST [70]. The basic structure of this MOF is composed of dimeric metal units interconnected by four BTC ligands (Figure 1) [71]. Some of the characteristics of this MOF are that it has an acceptable

surface area, pore volume and a good thermal stability, and reversible adsorption and desorption properties without signs of damage to the crystal structure [72,73]. In fact, it is reported in the study of Forsyth et al. [74], that it is considered as one of the most studied MOFs for this type of synthesis and has been tested under a variety of conditions in traditional solvents.

One point to note is that there is a lack of information on the wastewater treatment of the removal of persistent organic pollutants in aqueous media with HKUST-1. Thus, the unmodified HKUST-1 was not used between 2018 and 2022 for this type of contaminant. In fact, in this period, only studies have been found, such as that of Zhang et al. [75], which used this type of MOF for rhodamine B removal by photocatalytic degradation. Therefore, to remove persistent organic pollutants it is necessary to make modifications to HKUST-1. In this sense, Pan et al. [76] modified HKUST-1 by carbonization at a temperature of 350 °C under an oxygen-free atmosphere, which they called HDC-350. Upon characterization, this new material showed very different properties from those of the starting MOF. In fact, the great difference in the hydrophobicity of each of the MOFs was highlighted. In this case, HDC-350 had a higher hydrophobicity than HKUST-1, which may have been due to the loss of hydrophilic functional groups on the surface. Therefore, with these new characteristics of HDC-350, a great improvement in the adsorption of tetracycline was obtained. Another function of this type of MOF is coating nanoparticles, wherein the MOF gives the nanoparticles new properties. A very clear example is the work carried out by Wu et al. [77] by the addition of this MOF to nanoparticles, which in this case were cubic. Through this procedure, the nanoparticles were able to increase the carrier density and accelerate the interfacial charge separation and transfer. As a result of this procedure, the concentration of tetracycline hydrochloride was reduced up to (removal of around 93.40%) in 1 h under visible light irradiation. Another example of nanoparticle coating was reported by Wu et al. [78] that combined MOF with Fe<sub>3</sub>O<sub>4</sub> nanoparticles to improve the adsorption of certain pollutants. Using ciprofloxacin and norfloxacin, they found that adsorption was primarily due to electrostatic interactions and  $\pi$ - $\pi$  interactions.

Another alternative is to immobilise HKUST-1 on membranes to carry out various separations of water compounds. Yang et al. [79] allowed the separation of *E. coli* from the aqueous medium by using the HKUST-1@lignocellulose nanofibrils (LCNFs) membrane, and that of Bai et al. [80], who separated the water contaminated by the dyes congo red and methylene blue by adsorption. In addition, both studies stated that the synthesized membranes had promising properties as they had excellent stability and were antifouling [79,80].

### 3. Fe-MOF Synthesis

In this section, each of the synthesis methods of these materials is explained, especially Fe-MOFs, due to their application as catalysts in several AOPs. Fe-MOFs provide a greater number of catalytic sites, allowing them to more effectively generate free radicals due to the iron extranuclear electrons undergoing hybridization during bonding. Hence, Fe-MOFs are crucial to the development of AOP systems, including photo-electrocatalytic Fenton reactions, photo and electrocatalytic processes, ozone oxidation and advanced oxidation systems containing sulphate radicals.

It is important to emphasize the complexity of the synthesis of MOFs since their elaboration depends on many parameters. Normally, these are divided into two classes: operational and compositional [81,82]. The most important operational factors are the temperature and pressure to which they are subjected in the synthesis reaction and the time taken for this reaction [81,82]. The other, but no less important, are the compositional parameters, in which pH, solvents and organic ligands used, etc., could be highlighted [81,82]. Small changes in some of these parameters can lead to different kinds of MOFs. In Figure 3, the different methods of synthesis of Fe-MOFs are shown and several related operational parameters are introduced.

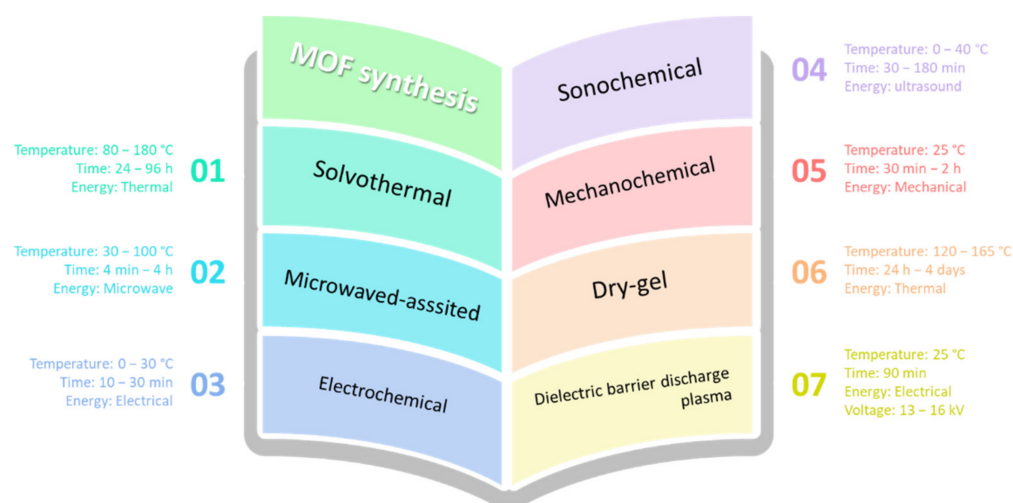


**Figure 3.** Most used synthesis methods to obtain Fe-MOFs [83].

Before starting to explain each of the methods shown in Figure 3, it is important to emphasise once again the importance of the chemical compounds involved, i.e., the source used to obtain the metal ions, in this case, the iron ions, the solvent and the organic ligand. As mentioned in Section 2.1, depending on the organic ligand and the metal ion used, a certain family of MOF (MIL, ZIF, etc.) can be obtained [84]. Despite this, the solvents used in the formation of MOFs play an important role in the distribution of the compounds since they are considered structure-directing agents or participate in the coordination of the structure with the metal ions [85]. Each of the synthesis methods will be explained with examples illustrating the components identified and operating conditions.

### 3.1. Solvothermal Synthesis

This synthesis technique consists of a chemical reaction, which takes place in a solvent at a temperature above the boiling point of the solvent and occurs at a pressure above 1 bar in a sealed vessel, commonly known as an autoclave [86,87]. In the case of MOFs, this synthesis involves a mixture of metal ions and organic ligands in a low solvent [88]. To obtain the synthesized MOFs, after the reaction in the autoclave, the obtained product needs to be filtered and dried by evaporation at room temperature [88]. Normally, the solvothermal method uses a highly soluble organic solvent such as acetonitrile, methanol, acetone or dimethylformamide (DMF) [88]. A major advantage of this method is that it can control particle size and shape distribution precisely by adjusting the reaction parameters [87,89]. Due to these characteristics, it is considered one of the most suitable and widely used conventional techniques for MOF synthesis [7]. In the following table, Table 4, some examples of Fe-MOF syntheses are shown.

The table reflects the procedure that is normally followed in several studies. As can be seen from this table and Figure 4a, the iron salt and the organic ligand are dissolved in a given solvent. When these reagents are completely released, the mixture is poured into a Teflon-lined steel autoclave reactor. This is placed in an oven in which a constant temperature is set for the duration of the reaction (Table 4). When the reaction is finished, the resulting solid is removed from the Teflon and then cleaned and dried.

During this synthesis, reagents, their counter anions, reaction time and temperature are mainly highlighted as the key factors. Thus, in the study of Mohammad et al. [90], three identical syntheses were carried out to obtain MIL-100 (Fe) but the iron salt used changed ( $\text{FeCl}_3$ ,  $\text{Fe}(\text{NO}_3)_3$  and  $\text{Fe}_2(\text{SO}_4)_3$ ) and the effect of these counter anions was evaluated. Although the characterisation of these materials was approximately similar, there were some differences in their photocatalytic activity. So, this shows the great complexity of the synthesis of Fe-MOFs.

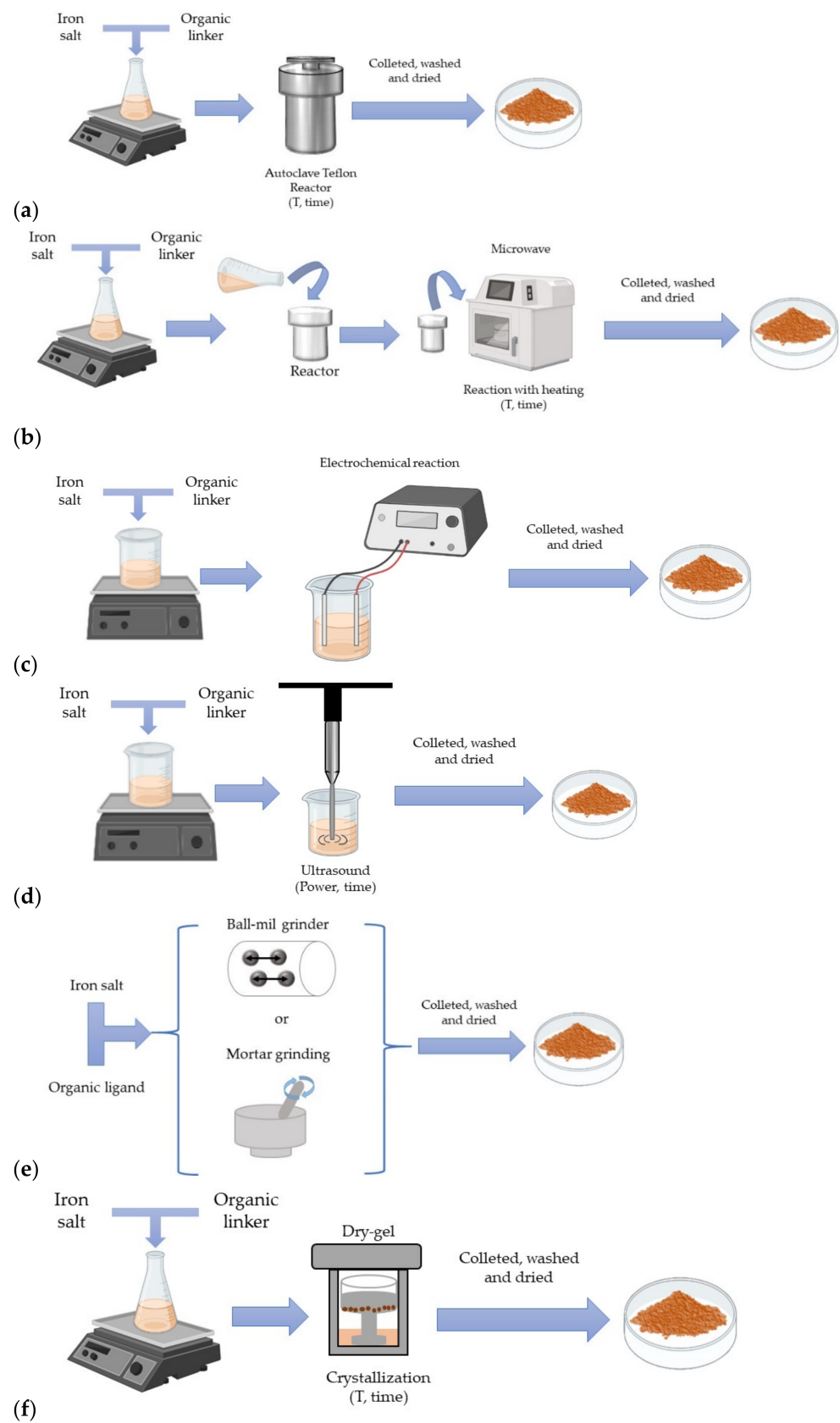


**Figure 4.** General scheme of (a) solvothermal/hydrothermal synthesis, (b) microwave-assisted synthesis, (c) electrochemical synthesis, (d) sonochemical synthesis, (e) mechanochemical synthesis, (f) dry-gel synthesis.

Moreover, the solvothermal method allows the synthesis of a wide variety of Fe-MOFs. Moreover, without altering the overall process of the method, it allows for the easy addition of modifications to the Fe-MOFs, and even the addition of another metal salt, as shown in the work of Wang et al. [91] who synthesized a cobalt–iron bimetallic MOF. This study demonstrated that the Fe-MOF had  $\text{Co}^{2+}$  in its structure as they analysed the 3D structure and detected that the Fe/Co-MOFs presented a herringbone ball shape due to the new coordination that had originated.

The synthesis process, despite its complexity, has proven viable and growing, as shown in Table 4. Consequently, it is an advance in the synthesis of bimetallic iron catalysts with another metal, improving the catalytic properties of Fe-MOFs in water decontamination processes.

### 3.2. Microwave-Assisted Synthesis

In general, microwave-assisted synthesis is based on the alignment of the dipoles of the material in an external field through the excitation produced by microwave electromagnetic radiation [92]. In addition, it has great characteristics compared to other MOF synthesis techniques: it is one of the fastest processes since the crystal nucleation is very fast; its heating is homogeneously distributed and it is environmentally sustainable [93–95]. Moreover, due to the type of heating and the short reaction times, it obtains more uniform crystalline particles with a larger surface area. It should be noted that it is easier to control the sizes of the crystals synthesized by this method, they are more repeatable, have a higher percentage yield in production and require smaller volumes of solvent to obtain them [96]. In this Table 5, some examples of Fe-MOF syntheses are given to show how to proceed.

As can be seen in Figure 4b, as in solvothermal synthesis, the reagents are first mixed, then incorporated into the reactor and subjected to certain conditions of temperature, time and power of the microwave equipment. The last step is purification to obtain the synthesized catalyst. With this general idea of the process, it should be noted that the Fe-MOFs found in the literature have been mostly unmodified MOFs, as in the work of Mahmoud et al. [97] or with functionalisation of the amino group, as in the work of He et al. [98].

**Table 4.** Examples of solvothermal/hydrothermal synthesis of Fe-MOF.

MOF	Organic Ligand	Metal Source	Solvent	Procedure	Reference
MIL-100-1	Trimesic acid ( $\text{H}_3\text{BTC}$ )	$\text{FeCl}_3$	Water	$\text{H}_3\text{BTC}$ and $\text{FeCl}_3$ (molar ratio 1:1) were mixed and transfer in a Teflon autoclave and placed in an oven (200 °C, 8 h). After cooling at room temperature, it was purified and dried at 80 °C under a vacuum overnight.	[90]
MIL-100-2	$\text{H}_3\text{BTC}$	$\text{Fe}(\text{NO}_3)_3$	Water	$\text{H}_3\text{BTC}$ and $\text{Fe}(\text{NO}_3)_3$ (molar ratio 1:1) were mixed in water following the same procedure as MIL-100-1.	[90]
MIL-100-3	$\text{H}_3\text{BTC}$	$\text{Fe}_2(\text{SO}_4)_3$	Water	$\text{H}_3\text{BTC}$ and $\text{Fe}_2(\text{SO}_4)_3$ (molar ratio 1:1) were mixed in water following the same procedure as MIL-100-1.	[90]
Fe/Co-MOF-x	Terephthalic acid (BDC)	$\text{FeCl}_3 \cdot 6\text{H}_2\text{O}$ and $\text{CoCl}_2 \cdot 6\text{H}_2\text{O}$	DMF	Metal ions ( $\text{Fe}^{3+}$ and $\text{Co}^{2+}$ ) and BDC were dissolved in DMF with a molar ratio of 1:1. Once NaOH solution was added, it was put in an oven at 100 °C for 10 h. When the reaction was completed, the resulting solid was recovered, cleaned and dried in a vacuum oven at 60 °C.	[91]

Table 4. Cont.

MOF	Organic Ligand	Metal Source	Solvent	Procedure	Reference
MIL-53(Fe)-NH <sub>2</sub>	2-aminoterephthalic acid (NH <sub>2</sub> -BDC)	FeCl <sub>3</sub> ·6H <sub>2</sub> O	HCl	A reaction mixture of NH <sub>2</sub> -BDC, HCl and FeCl <sub>3</sub> ·6H <sub>2</sub> O (molar ratio 1:1:1) was loaded in a 10 mL glass vial, sonicated for 1 min in an ultrasound bath and placed in a microwave. Then, it was heated to the reaction temperature as fast as possible with different power impulses. Then, it was cooled down to 65 °C by an airflow. The resulting product was washed.	[99]
Fe-MOF	BDC	FeCl <sub>3</sub> ·6H <sub>2</sub> O	DMF	FeCl <sub>3</sub> ·6H <sub>2</sub> O and BDC (molar ratio 1:1) were dissolved in 50 mL DMF. Then, 10 mL NaOH solution was added. Then it was placed in an oven at 100 °C for 10 h. After the reactor cooled, the resulting solid was recovered, cleaned and dried in a vacuum oven at 60 °C.	[91]
Fe-MOF	H <sub>2</sub> BDC	FeSO <sub>4</sub> ·7H <sub>2</sub> O	DMF	A total of 20 mL DMF with H <sub>2</sub> BDC (2.6734 g) was stirred for 30 min, while FeSO <sub>4</sub> ·7H <sub>2</sub> O (3.2133 g) was dissolved in 20 mL of deionized water. Then both dissolutions were mixed and stirred for 30 min, and then transferred to the reactor (150 °C for 12 h). Finally, the product was filtered, washed and dried (70 °C for 5 h).	[100]
Zr/Fe-MOFs/GO	BDC	FeSO <sub>4</sub> ·7H <sub>2</sub> O and zirconium acetate	DMF	A hydrothermal process was used to synthesize the compound. Two solutions, BDC and DMF (ratio: 3.3215 g:10 mL) and FeSO <sub>4</sub> ·7H <sub>2</sub> O and zirconium acetate. (ratio: 2.8133 g:2.6 mL) were mixed and transferred to a reactor (120 °C for 10 h). Then, the reaction mixture was filtered, washed and dried (80 °C for 12 h).	[101]
Mg/Fe-MOF	BDC	Fe(NO <sub>3</sub> ) <sub>3</sub> ·9H <sub>2</sub> O and MgCl <sub>2</sub> ·6H <sub>2</sub> O	DMF and acetonitrile	Fe(NO <sub>3</sub> ) <sub>3</sub> ·9H <sub>2</sub> O, MgCl <sub>2</sub> ·6H <sub>2</sub> O and BDC (molar ratio 10:1:12.4) and 40 mL DMF were mixed. Next, 40 mL of acetonitrile was added and the mixture was placed into a Teflon flask in an oven (150 °C for 12 h). After cooling, the precipitate was collected, washed and dried at 150 °C under a vacuum.	[102]
Cu/Fe-MOF	BDC	Fe(NO <sub>3</sub> ) <sub>3</sub> ·9H <sub>2</sub> O and Cu(NO <sub>3</sub> ) <sub>2</sub> ·3H <sub>2</sub> O	DMF and acetonitrile	Fe(NO <sub>3</sub> ) <sub>3</sub> ·9H <sub>2</sub> O, Cu(NO <sub>3</sub> ) <sub>2</sub> ·3H <sub>2</sub> O and BDC (molar ratio 10:1:12.4) and 40 mL DMF were mixed. Next, 40 mL of acetonitrile was added and the mixture was placed into a Teflon flask in an oven (150 °C for 12 h). After cooling, the precipitate was collected, washed and dried at 150 °C under a vacuum.	[102]

Table 4. Cont.

MOF	Organic Ligand	Metal Source	Solvent	Procedure	Reference
MIL-100(Fe)/rGO	H <sub>3</sub> BTC	Fe(NO <sub>3</sub> ) <sub>3</sub> ·9H <sub>2</sub> O	Water	Fe(NO <sub>3</sub> ) <sub>3</sub> ·9H <sub>2</sub> O (14.43 g) and H <sub>3</sub> BTC (5.04 g) were dissolved in water (36 mL). The rGO (50 mg) was dispersed in distilled water (100 mL) under ultrasonication for 1 h, and both dissolutions were mixed for 1 h. Then it was transferred to a Teflon-lined stainless-steel autoclave (150 °C for 15 h). After that, the product was collected, washed and dried at 90 °C overnight.	[103]
Cu-doped MIL-101(Fe)	H <sub>2</sub> BDC	FeCl <sub>3</sub> ·6H <sub>2</sub> O and Cu(OAc) <sub>2</sub>	DMF	A total of 1.35 g of FeCl <sub>3</sub> ·6H <sub>2</sub> O, 415 mg of H <sub>2</sub> BDC and 181.6 mg of Cu(OAc) <sub>2</sub> were added to 30 mL of DMF. Then it was transferred to a Teflon-lined autoclave and left at 110 °C for 20 h with a heating rate of 5 °C/min. After the reaction was over, the solid product was collected, washed and dried at 80 °C overnight.	[104]

Among the modified MOFs, the Fe-MOF synthesized by Li et al. [105] was the Fe<sub>3</sub>O<sub>4</sub>@MIL-100(Fe). This MOF, unlike all the others found by this synthesis method, used Fe<sub>3</sub>O<sub>4</sub> nanoparticles, which were previously synthesized by the solvothermal method, as the magnetic core of the Fe-MOF. By making this change, a material with a high adsorption capacity of ciprofloxacin (273.65 mg/g) and with high selectivity was obtained. As for the unmodified Fe-MOFs, they stand out because they do not use any solvent, they only use the iron salt with a certain ligand providing a green approach to the synthesis. This is important because no toxic solvents are used, such as DMF, and less waste or by-products are generated.

To improve the properties that Fe-MOF can exhibit, a combination with other synthesis methods has been proposed. Common examples that have been found include microwave-assisted hydrothermal synthesis, which allows the advantages offered by microwave and hydrothermal methods [106] and the combination of microwave and solvothermal methods [107]. These combinations of methods are not considered in Table 5.

### 3.3. Electrochemical Synthesis

Regarding this type of synthesis, it is considered contrary to the solvothermal method, since it does not use high pressures and temperatures which are associated with high energy requirements, but rather operates under ambient conditions [108]. By using this synthesis method, the metal ion is provided through anodic dissolution in a synthesis mixture that includes organic linkers and electrolytes [109]. To carry out this synthesis, the following components are needed: an anode, a power supply and cathode plates. Normally, the assembly is very simple and does not require anything specific as it is only necessary that the anode and cathode are immersed in an electrochemical medium, in which both the metal salt and the organic ligands are included [110]. To clarify the idea of this synthesis method, Figure 4c shows a schematic representation of the general procedure followed. Therefore, in electrochemical synthesis, the most important parameters for MOF synthesis are the solvent, the applied voltage, the electrolyte and the temperature at which the synthesis is carried out.

Similarly to microwave synthesis, this synthesis also takes a short amount of time [111], but unlike the others, it is the alternative that best solves the continuous production of these catalysts. In general, this type of synthesis method has attracted more interest because it provides the ability to synthesize MOF thin films or MOF-coated electrodes. This can

occur if the desired substrate is deposited directly or indirectly on that surface. Thus, this allows the adjustment of the MOF structure and control of the MOF characteristics. Taking this into account, direct and indirect electrosynthesis must be differentiated [112]. The main difference between both of them is that in the indirect methods the electrochemical process is carried out in a single step in the overall procedure of MOF synthesis, while in direct synthesis, this catalyst has already been obtained with only this electrochemical process [113]. Briefly, in direct synthesis, anodic dissolution and reductive electrosynthesis stand out, while in indirect synthesis, bipolar electrosynthesis, electrophoretic deposition and galvanic displacement stand out [112].

**Table 5.** Examples of Fe-MOF that were synthesized by the microwave-assisted method.

MOF	Organic Ligand	Metal Source	Solvent	Procedure	Reference
Fe <sub>3</sub> O <sub>4</sub> @MIL-100(Fe)	H <sub>3</sub> BTC	Fe <sub>3</sub> O <sub>4</sub> nanoparticles	Water	H <sub>3</sub> BTC (1.0 g), Fe <sub>3</sub> O <sub>4</sub> microspheres (0.6 g) and water (12.5 mL) were reacted under microwave at 150 °C for 30 min (300 W). The solid was collected, washed and dried in a vacuum at 60 °C.	[105]
NH <sub>2</sub> -MIL-101(Fe)	NH <sub>2</sub> -BDC	FeCl <sub>3</sub> ·6H <sub>2</sub> O	DMF	Dissolved FeCl <sub>3</sub> ·6H <sub>2</sub> O and acetic acid in DMF under sonication, followed by the addition of NH <sub>2</sub> -BDC. Then, it was placed in a microwave reactor (110 °C and 45 min). After that, the reactor was cooled down to room temperature, the precipitates were collected, cleaned and finally dried under vacuum at 60 °C overnight.	[114]
MIL-88A(Fe)	Fumaric acid	FeCl <sub>3</sub> ·6H <sub>2</sub> O		The fumaric acid solution was added into a FeCl <sub>3</sub> ·6H <sub>2</sub> O solution (ratio molar 1:1). Then it was transferred into a microwave oven and heated for 3 min. Finally, the formed precipitate was collected, washed and dried at 70 °C.	[97]
Fe-MOFs	H <sub>3</sub> BTC	FeSO <sub>4</sub> 7H <sub>2</sub> O		FeSO <sub>4</sub> 7H <sub>2</sub> O and H <sub>3</sub> BTC (with a ratio molar of 1.5:1), stainless-steel balls and deionized water were combined in a tetrafluoroethylene milling pot. Stir milling was performed at 200 rpm and the microwave oven was started concurrently for 40 min. The solid was filtered, washed, added to a beaker containing ethanol and then stirred with a magnetic stirrer for 3 h. This mixture was then filtered and dried.	[115]
NH <sub>2</sub> -MIL-88B(Fe)	NH <sub>2</sub> -BDC	FeCl <sub>3</sub> ·6H <sub>2</sub> O	DMF	FeCl <sub>3</sub> ·6H <sub>2</sub> O, NH <sub>2</sub> -BDC and DMF (molar ratio of 1:1:282) were mixed for 30 min and the solution was degassed by shaking in an ultrasonic bath for 5 min. Then, it was transferred into a Teflon autoclave and placed in a microwave oven (150 °C, 20 min and 600 W). The final product was purified and dried under a vacuum at 60 °C overnight.	[98]

Based on what has been mentioned above, the great complexity of this method can be noted as well as the fact that not all metals have been used to synthesize MOFs. Of all those found, Cu-, Ti- and Zn-MOF are the ones that stand out [116]. Nevertheless, in recent years, more and more articles have started to use this method to obtain Fe-MOF. In fact, the first work that synthesized Fe-MOFs by this method was performed by Campagnol et al. [117] in 2013. Since then, these MOFs have been gradually synthesized using this method. Therefore, it is relevant to mention some of these remarkable works. The first of these works was the one by Wu et al. [118], in which they managed to synthesize Fe-MIL-101 and Fe-MIL-101-NH<sub>2</sub> in 30 min. In addition to being a fast method, they produced crystals of these MOFs with properties, such as a high surface area, comparable to those obtained by the solvothermal method, in which the operating conditions are more aggressive. Concerning the study of Zhang et al. [119], a metal–organic nanocomposite was fabricated by cathodic electrodeposition and the main novelty of this synthesis was that it was carried out in a single step. Furthermore, they carried out its characterisation and found that the variation in the morphology, structure and electrochemical activity of the Fe-BTC film was closely related to the redox state of the iron ions in the electrosynthesis process.

### 3.4. Sonochemical Synthesis

Sonochemical synthesis is based on the application of high ultrasonic energy. It consists of cyclic mechanical vibration and possesses a frequency between 20 kHz and 1 MHz that allows the chemical reaction to occur (Figure 4d) [120]. In fact, the key part of this synthesis is the generation, growth and collapse of a bubble that occurs in the aquatic environment [121]. This process is known as acoustic cavitation and features very high local temperatures and pressures with a very large cooling and heating rate [121]. As for their characteristics, similar to other synthesis methods, they are also able to provide homogeneous nucleation, decrease crystallisation time and have low energy consumption [120,121]. In addition, another advantage of this method is that the preparation of the components uses ambient conditions and is energy efficient, making it a process that can be considered environmentally friendly [122]. Because of all these advantages and its extensive use in the synthesis of nanoparticles, it has started to be used in the synthesis of MOFs [122].

Although it is considered an environmentally sustainable method, it should not be forgotten that some syntheses use toxic solvents such as DMF; an example of this is the work of Abdpour et al. [123], who carried out the synthesis of a novel MIL-100(Fe)@MIL-53(Fe) photocatalyst. This catalyst has very favourable properties as it allows the degradation of a dye such as methyl orange and its reuse with a degradation efficiency remained around 92% in the fifth cycle [123]. However, there is evidence of the influence of the solvents used in the synthesis and this fact is reflected, for example, in the work of Hossein Zadeh et al. [124]. They studied the photocatalytic properties of their synthesized MOF, which was Fe-benzentricarboxylic (Fe-BTC), depending on the combination of solvents used (DMF, distilled water and ethanol). From this study [124], they concluded the existence and importance of this influence and the need to use DMF.

Nevertheless, other studies have looked for alternatives to having free Fe-MOF to see if they could improve the existing Fe-MOF or use no-toxic dissolvent. Indeed, this was achieved and a clear example was the work of Taherzade et al. [125], who immobilized MIL-100(Fe) in carboxymethylated cellulose (CMC). A great advantage of their synthesis was that the solvent used was water, so proving non-toxic solvents can be used, and it operated under non-severe conditions. The only drawback was the long drying time of the final product which was 7 h at a temperature of 60 °C. Despite this drawback, this synthesis is promising as it achieved better adsorption rates and was more efficient than MIL-100 (Fe) which was synthesized by the solvothermal method [125].

Finally, similar to the microwave synthesis route, this method has also been widely used in combination with other methods to enhance the advantages provided by both

methods combined. Examples include sonochemical-assisted hydrothermal synthesis [126] and the combination of microwave and sonochemical [127].

### 3.5. Mechanochemical Synthesis

The name of this type of synthesis is related to the fact that the chemical reaction that takes place to obtain the MOF is mainly due to the application of mechanical energy (Figure 4e) [128]. The main characteristics of this synthesis route are that the obtained MOF has a highly crystalline structure, the operating conditions are mild as it is at ambient conditions, the reaction times are relatively short, less than one hour, there is no waste generation and it is economical and environmentally friendly as it does not use a solvent or a small amount of it. It is also considered a synthesis route with a wide field of application due to its ability to synthesize various archetypal MOFs [129,130].

It should be noted that this technique can be classified into Neat grinding (NG), Liquid-assisted grinding (LAG) and ion-and-liquid assisted grinding (ILAG) [131,132]. The difference between the three classes is that NG uses no solvent at all, LAG uses a small amount of solvent and ILAG, in this case, uses solvents with traces of salt additives [133]. Similar to LAGs, this concept incorporates both liquid and salt, which makes it different from LAGs. The reason for adding these salts is that they promote the dissolution of the solid reagents and this implies a better homogeneous mixing of the reaction and, thus, improves the efficiency of the process as well as the quality and selectivity of the MOFs if the additives are chosen in a suitable way. It should be noted that this method is quite recent since the first reported study in which a Fe-MOF was synthesized was in 2015 by Pilloni et al. [134]. Since that year, researchers have published on the synthesis of these MOFs by the mechanochemical method. A clear example of the progress in this technique and the advantages that this synthesis can provide to obtain catalysts is the MOF synthesized by Jeong et al. [135]. They highlighted that Fe-MIL-88A was synthesized by the NG method in only 10 min, and had a specific surface area five times larger than when the same MOF was produced by the solvothermal method [135].

He et al. [136] synthesized a Fe-Pd@C nanomaterial to remove phenol by a Fenton process and compared it with the commercial version of Fe/C material. This material was synthesized by the mechanochemical method and subsequent carbonisation. In the degradation tests, they obtained promising results as the catalyst by the Fenton process could remove up to 95% of the phenol in 1 h and the iron leaching was very low, 0.05%. Therefore, they were able to state that this synthesized catalyst presented an excellent catalytic performance and had a good stability, and they proved that it could also be reused in this removal process [136].

### 3.6. Dry-Gel Synthesis

This type of synthesis is characterized by its ability to produce porous materials from low amounts of reagents, reducing the generation of waste and allows the MOF to also be produced continuously [137]. In addition, this method enables the reuse of the solvent for multiple synthesis cycles without compromising the yield and quality of the crystals formed [83]. Figure 4f shows a schematic representation to better understand what this method consists of.

Ahmed et al. [138] reported the first Fe-MOF synthesized by this technique in 2012. Among the most recent studies conducted in this line, we can highlight the work by Luo et al. [139] and Tannert et al. [140]. Luo et al. [139] synthesized MIL-100 (Fe) with a hierarchical pore structure and in the absence of liquid solvents, obtained yields by the dry-gel method 85% higher than the traditional hydrothermal method (76%). Additionally, the operating conditions were also more favourable for the dry-gel method. Tannert et al. [140] synthesized the same catalyst, MIL-100 (Fe), but by the microwave-assisted dry-gel method. The results were favourable because the reaction times were considerably shortened to 3 h, compared to 24 h requested by Luo et al. [139]. Thus, the integration of microwave in the dry-gel method helps to reduce the synthesis time obtaining MOFs of similar characteristics.

### 3.7. Other Synthesis Methods of Fe-MOF

In addition to the most commonly used synthesis methods for Fe-MOF synthesis described above, it is also known that other methods are relevant, such as spray drying synthesis, continuous flow synthesis and the dielectric barrier discharge (DBD) plasma method.

Regarding the spray drying technique, it is characterized mainly by the fact that it is a simple and fast method, with a considerable reduction in the generation of waste [83] and also allows the recovery of the used solvent, so it is considered a very sustainable synthesis method. A noteworthy aspect of this synthesis method is the crucial parameter used to intrude the reagents into the reaction system [141]. In fact, this parameter can affect the morphology and the characteristics of the synthesized Fe-MOF. Garzon-Tovar et al. [142] reported a 78% yield of Fe-BTC/MIL-100 synthesis by the optimization of this method and the integration of a continuous-flow reactor at the entrance of the spray-dryer to induce nucleation before spray-drying. In addition to improving the synthesis yield of Fe-MOF, they were the first to develop this technology, which they called continuous flow-assisted synthesis.

Continuous flow synthesis is mainly used in the synthesis of functional nanomaterials and can be a tool for large-scale Fe-MOF synthesis [83]. Employing a continuous flow of reagents, which go through maintained pipes or coils, allows for rapid crystal formation as this nucleation is favored by a higher surface-to-volume ratio at the reaction temperature. Le et al. [143] synthesized MIL-100(Fe) by the microwave-assisted continuous flow method and achieved a production rate of  $771.7 \text{ kg}\cdot\text{m}^3/\text{d}$ . In addition, this continuous produced Fe-MOF showed a better crystallization and potency than the ones synthesised by batch process.

Finally, the DBD plasma method is a novel MOF synthesis technique that is low-cost and is considered as environmentally sustainable [144]. This synthesis method is based on the electrical discharge between two electrodes separated by an insulating dielectric barrier. The procedure carried out in this synthesis method is depicted in Figure 5. Tao et al. [145] were the first to report this synthesis route that provided several advantages such as the reduction in synthesis time and enhanced the adsorption properties of the catalyst. Since then (2019), only six papers have been published, based on Scopus databases about Fe-MOF synthesis with this method [144–149]. Therefore, it is possible that in the not-too-distant future, this method will be used more frequently for the synthesis of Fe-MOF. In addition, the appearance of this method opens the door to possible new methods, which coexist with all the methods mentioned above.

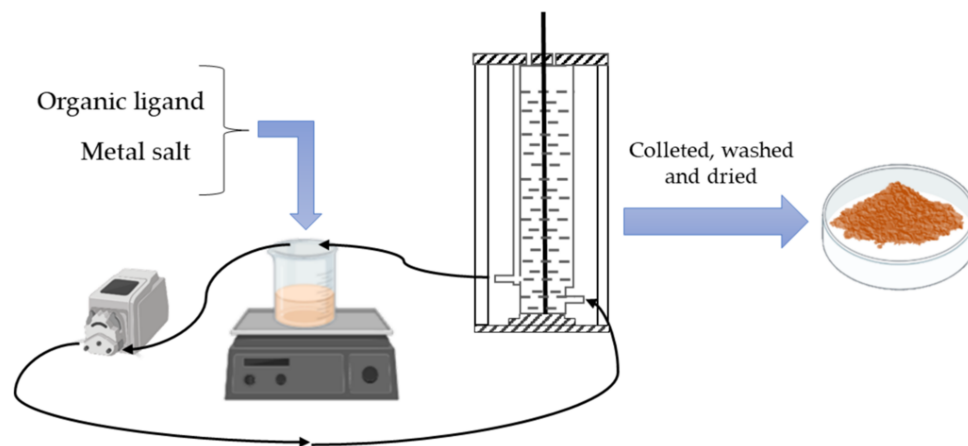


Figure 5. Schematic of the procedure found in papers using this synthesis technique.

## 4. Application of Fe-MOF in Advanced Oxidation Processes

AOPs can be divided according to the type of reaction involved or to the process underlying as shown in Figure 6 [150,151]. The catalytic processes are based on the Fenton reaction, in which the hydroxyl radicals are generated through the use of iron and hydrogen peroxide (Equation (1)) [152]. Similar to the conventional process, the Fenton-like process

can generate powerful oxidants, replacing iron by transition metals [153] or generate sulphate radicals following the reactions shown in Equations (2) and (3) [154].

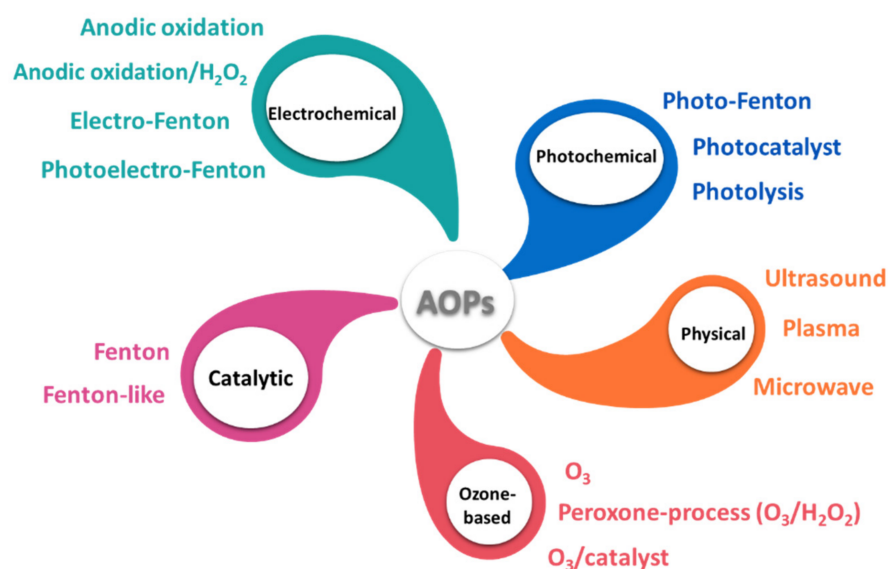
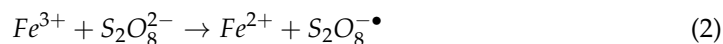
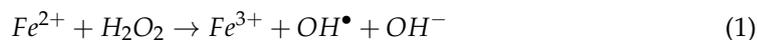


Figure 6. Classification of AOP by the fundamentals of the process itself.

However, there are some drawbacks to using these catalysts, particularly the acid pH regulation, sludge generation and the loss of catalyst in the effluent. Several heterogeneous AOPs, with a wide variety of materials as catalysts or supports, have been reported to overcome these drawbacks. Despite the homogeneous catalyst disadvantages, the reaction rate is higher than in heterogeneous systems, which require an increase in the catalyst surface area [155,156]. Thus, it is critical and challenging to develop new catalysts with low cost, high activity, and good chemical stability. Among them, MOFs have stood out in the last ten years.

The same trend was observed when reviewing the Scopus database for a period of five years (2018 to 2022) using the keywords: “metal-organic frameworks”, “advanced oxidation processes” and “wastewater”. An analysis of the co-occurrences of keywords using bibliographic network maps from VOS Viewer® is shown in Figure 7. The figure below illustrates the co-occurrence network of the top 29 most frequently occurring keywords. Each node represents a keyword, and each line represents the co-occurrence relation between them. Moreover, the results were normalized using fractionalization, which is commonly employed to normalize the strength of the links between items.

As shown in Figure 7, the color of each node (keyword) corresponds to its average year of appearance. Before 2020, the number of MOF studies in this field was insignificant. Therefore, there are no nodes with the color purple, which represents the papers reported in 2018, and the only keyword in 2019, which is in dark blue, is synthesis. The number of keywords used after 2020 increased very rapidly, and it is possible to see the evolution of different AOPs over time.

As shown in the previous sections, the synthesis of these Fe-MOFs is crucial for obtaining some of the properties of these catalysts that are of particular interest for the development of different AOPs. Based on the current interest, this article will focus on the application of MOFs in several AOPs such as Fenton, electro-Fenton, photocatalysis and mainly those focused on the use of Fe-MOF as a catalyst.

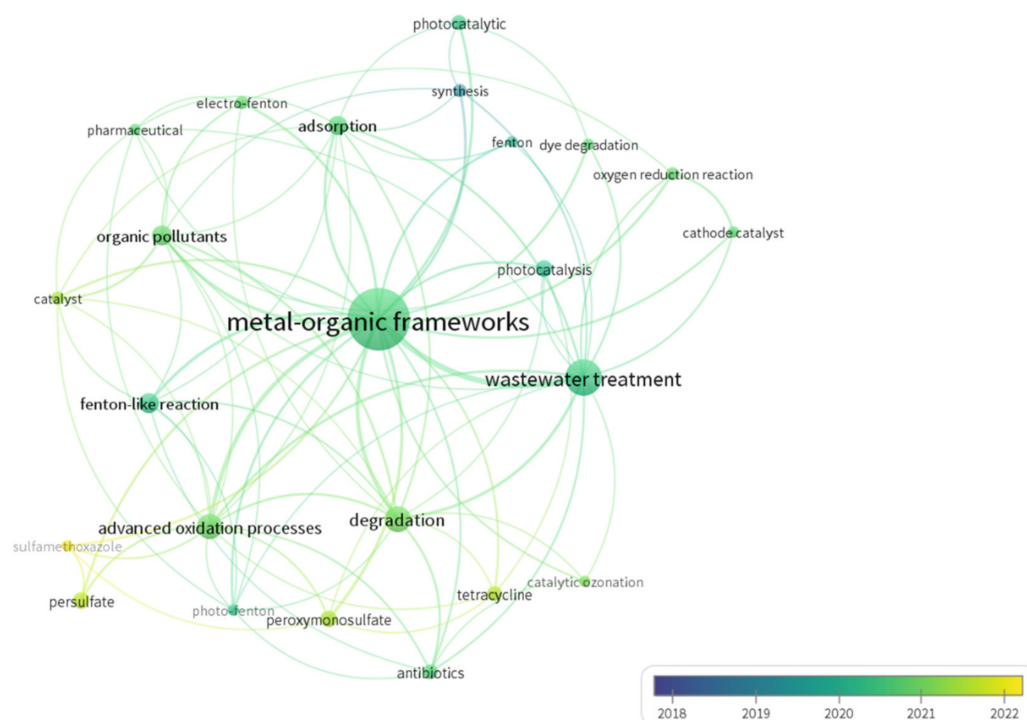


**Figure 7.** Keywords and overlay visualization co-occurrence analysis of AOPs using MOFs in wastewater research using VOS Viewer®.

#### 4.1. Catalytic AOP

Some examples of various Fe-MOFs synthesized for the application of Fenton-based processes are shown in Table 6. Until now, Fe-MOFs from the MIL family (such as MIL-100-Fe, MIL-88-Fe and MIL-53-Fe) have demonstrated great interest and potential as Fenton catalysts because of their ease of synthesis, large surface area and high chemical stability [157]. Liao et al. [158] synthesized by the solvothermal process three types of MIL-88A-Fe with different morphologies (rod, spindle and diamond). They concluded that the catalyst morphology affected the efficiency of the Fenton-like process. Thus, using rod-MIL-88A-Fe (r-MIL-88A-Fe) as a catalyst, phenol could be completely removed by the Fenton process with degradation levels higher than other reported Fe-based such as MIL-53-Fe, MIL-88B-Fe and MIL-101-Fe [159]. This fact could be explained by the DFT calculation that suggested the hydroxyl radical was more easily generated due to a lower  $H_2O_2$  dissociated energy barrier. In addition, the high surface of rod configuration increased the phenol removal. Moreover, the r-MIL-88A-Fe performance should be reusable for practical applications. In this sense, only a slight decline in r-MIL-88A's activity was detected, which indicates that this catalyst is highly reusable.

Among the studies shown in Table 6, it is highlighted the Fe-MOF (core/shell Fe@C nanocomposites) was synthesized via a green technology by the combination of a mechanochemical approach and carbonization under an inert atmosphere. In this study, He et al. [136] included a trace of Pd by addition of  $Na_2PdCl_4$  into the Fe-MOF, determining a positive effect on the pH endurance, life of modified catalyst and reduction in the generation of iron sludge. In addition, catalysts were re-used after they were recovered from reaction mixtures in the successive runs to verify their stability and operational limitation. As a result of their high magnetization, the catalysts could easily be recovered under an external magnetic field, showing a high level of phenol degradation decreasing around 70% after several cycles. This reduction in efficiency could be due to the metals leaching; however, there was a low and constant concentration (lower than 3 mg/L) of Fe and no Pd ions were present in the different cycles. These results suggest that the catalyst's life was extended, and metal sludge was reduced, thereby enabling the discharge of treated effluents directly into the environment.

Fe@MesoC is another magnetic catalyst that has been synthesized from MIL-100-Fe by the pyrolysis/carbonization method and used as a catalyst in the Fenton process by degrading sulfamethoxazole (SMX) [160]. Similarly, the direct thermal treatment of MOFs holds great promise for constructing various metal oxide nanoparticles encapsulated inside porous carbon matrixes, providing compositions and structures tailored to the treatment's needs. As is shown in Table 6, the complete decomposing of SMX was achieved after two hours with only around 55% of total organic carbon removal. It could be due to the amelioration of the mesoporous carbon matrix or the abundance of active iron sites in the nanoparticles that this outstanding performance is possible. In addition, the electrons transfer from  $\text{Fe}^0$  to iron oxide could enhance the reduction of ferric to ferrous iron anchored to the surface of the catalyst ( $\equiv\text{Fe}^{3+}$  to  $\equiv\text{Fe}^{2+}$ , respectively) facilitating the redox cycle and the hydroxyl radical production.

Recently, the bimetallic MOFs have been probed as Fenton-like catalysts. Thus, Tang et al. [161] synthesized a bimetallic MOF, named  $\text{Fe}_x\text{Cu}_{1-x}(\text{BDC})$ , by the solvothermal method explained in Section 3.1. In this case, the DMF solution contained  $\text{FeCl}_3 \cdot 6\text{H}_2\text{O}$ ,  $\text{Cu}(\text{NO}_3)_2 \cdot 3\text{H}_2\text{O}$  and  $\text{H}_2\text{BDC}$ . The molar ratio of Fe/Cu in the catalyst was adjusted in the function of the ratio of the two metallic precursors, obtaining several bimetallic MOFs with a different initial molar ratio of Fe/Cu. The best SMX degradation was obtained using a ratio Fe/Cu of 0.75/0.25 at pH around 5.6. This catalyst overcame one of the limitations of the Fenton reaction that requests acid conditions. The results clearly show that this bimetallic MOF was effective at a wide range of pH from 4 to 8.6. As is shown in Figure 8 the presence of both metallic species on the catalyst surface served as active sites for  $\text{H}_2\text{O}_2$  activation and also to the generation of hydroxyl radicals increasing the efficiency of SMX degradation. By the use of this catalyst, the anchored  $\text{Fe}^{2+}$  ( $\equiv\text{Fe}^{2+}$ ) to the  $\text{Fe}_x\text{Cu}_{1-x}(\text{BDC})$  surface followed the reaction shown in Figure 8 and the lost electron to activate  $\text{H}_2\text{O}_2$  was captured by  $\equiv\text{Fe}^{3+}$  to form  $\text{HO}_2\bullet$  and regenerate  $\text{Fe}^{2+}$  (Figure 8). Similarly, the Cu active sites also catalyze the decomposition of  $\text{H}_2\text{O}_2$  and the same radicals were generated with the regeneration of  $\equiv\text{Cu}^{2+}$  to  $\equiv\text{Cu}^+$ . Thus, considering the standard reduction potentials of Cu (0.17 V) and Fe (0.77 V), part  $\text{Cu}^+$  generated on the  $\text{Fe}_x\text{Cu}_{1-x}(\text{BDC})$  surface could promote the regeneration of  $\text{Fe}^{2+}$  by a thermodynamically favorable electron transfer process (Figure 8), that increased the  $\equiv\text{Fe}^{2+}$  on the catalyst surface.

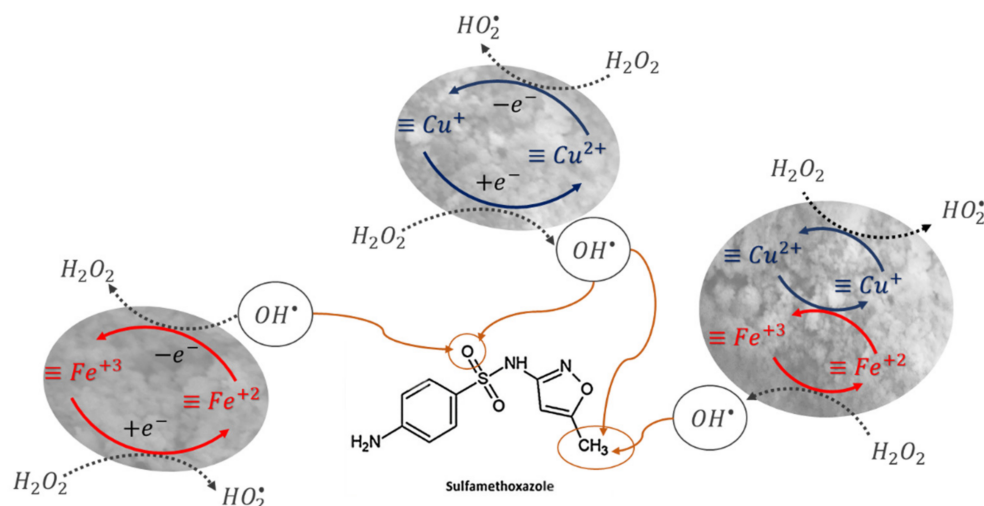
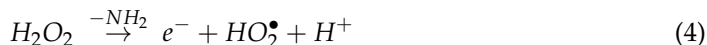


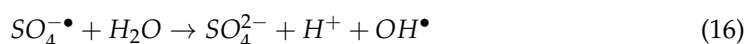
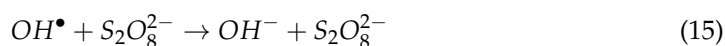
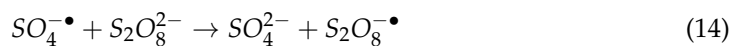
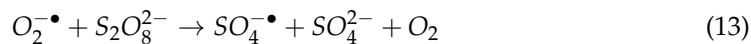
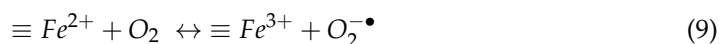
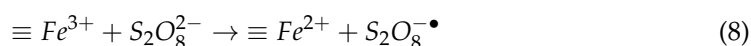
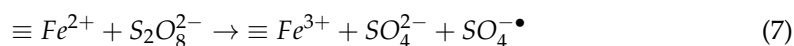
**Figure 8.** Graphical scheme of the reactions occurring on the  $\text{Fe}_x\text{Cu}_{1-x}(\text{BDC})$  surface for SMX degradation.

Recently, Huang et al. [162] explored the introduction of  $-\text{NH}_2$  groups as electron-rich donors to promote the cycling of  $\equiv\text{Fe}^{3+}$  to  $\equiv\text{Fe}^{2+}$ . They determined the reduction in the activation energy barrier in the dissociation of  $\text{H}_2\text{O}_2$  adsorbed on the surface of  $\text{Fe-BDC-NH}_2$  in relation to  $\text{Fe-BDC}$  due to the amino groups providing more electrons for hydrogen peroxide activation. The generation of hydroxyl radicals was also increased due to the direct injection of internal electrons (Equations (4)–(6)) that favor the reduction of  $\equiv\text{Fe}^{3+}$

generating more radicals ( $\text{OH}\bullet$  and  $\text{O}_2\bullet^-$ ) that attacked the target pollutants until the total mineralization.



The electron-donating properties of Fe-MOFs are likely to make them suitable for PS activation through Fenton-like reaction pathways. In Table 6, several studies in which Fe-MOFs were used as persulfate activators for the degradation of several pollutants are summarized. Pu et al. [163] evaluated the SMX degradation by different Fe-MOFs with cyclopentadienyl iron(II) dicarbonyl dimer  $[\text{Fe}(\text{Cp})(\text{CO})_2]_2$  as an iron precursor. In this study, different carboxyl group-containing pyridine compounds were used as organic ligands: Nicotinic acid (HNic), cinchomeric acid (Py-3,4-H<sub>2</sub>BDC), and 5-(pyridine-4-yl) isophthalic acid (H<sub>2</sub>PIP) obtaining three MOFs named as Fe(Nic), Fe(PyBDC) and Fe(PIP), respectively, by hydrothermal self-assembled coordination synthesis. They mentioned that the activation process was due to the reaction on the Fe-MOF surface ( $\equiv\text{Fe}^{2+}/\equiv\text{Fe}^{3+}$ ) and iron soluble form in water, with the heterogeneous process the main responsible for the activation reactions. Thus, it was detected that the  $\text{Fe}^{2+}/\text{Fe}^{3+}$  ratio of Fe(Nic) and Fe(PyBDC) decreased after activation, which indicates that  $\equiv\text{Fe}^{2+}$  acted as the electron donor for PS decomposition with  $\equiv\text{Fe}^{3+}$  generation reducing the surface activate sites (Equation (7)). However, for Fe(PIP) the ratio was similar, suggesting that the one-electron reduction of  $\equiv\text{Fe}^{3+}$  regeneration to persulfate anion took places (Equation (8)). Their studies also confirmed the coexistence of other radicals generated by several of the reactions showed in Equations (9)–(16) that contributed in the SMX degradation. Based on the characterization and degradation studies, it was determined that the different behavior of the synthesized Fe-MOFs was due to the organic ligands used that were capable of regulating the amount of  $\equiv\text{Fe}^{2+}$  active sites.



During the reuse experiments, it was observed that ferric oxide layers were formed on the surface blocking the active sites that reduced the reactivity of these catalysts in successive cycles. Thus, for real applications of these catalysts in wastewater treatment, it is essential to solve the sustainability and self-decomposition problems associated with Fe-MOFs that allow them to operate in a flow system with high activation capacities.

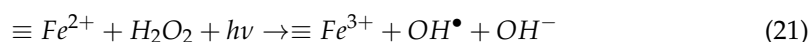
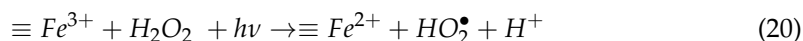
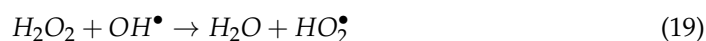
PBAs are a type of metal-containing coordination polymer that are considered a subset of the MOF and able to act as a catalyst in the PMS decomposition. Pi et al. [164], combined  $\text{Co}_3[\text{Fe}(\text{CN})_6]_2$ , and graphene oxide (GO) by a two-step hydrothermal procedure and obtained a Co-Fe PBAs@rGO nanocomposite. In contrast to the previous study with Fe-MOFs, in this case, in addition to the catalytic effect of anchored Fe, the capacity of Co was

added, being responsible for the activation of PMS. It was demonstrated that GO reduced the aggregation of the nanoparticles GO doped with nitrogen increasing the stability of the catalyst. However, Co and Fe were released to the bulk solution (lower than 1 mg/L) to reduce the metallic content on the catalyst in successive cycles. In addition, the reduction in catalytic activity of this bimetallic MOF could be also due to the adsorption of reaction intermediates that were attached to the catalyst surface.

#### 4.2. Photo-Based AOPs

The hydroxyl radicals could be generated by means of radiation, such as ultraviolet light (UV) or sunlight. Catalysts, also known as photocatalysts, are normally used to encourage this photochemical reaction to take place [165]. As a semiconductor material, it is defined by two separate energy bands: the highest energy band with electrons and the lowest without electrons, known as the valence and conduction bands, respectively [166]. The more common photocatalyst listed in the databases is TiO<sub>2</sub> (alone and modified), due to its great advantages such as low cost, low level of toxicity and thermal stability [165]. However, in recent years, other photocatalysts such as MOFs have been synthesized with similar results.

In 2007, the Corma group [167] evaluated the photocatalytic activity of MOF-5 (Zn<sub>4</sub>O(BDC)<sub>3</sub>) for phenol degradation under UV light irradiation, confirming the low stability of this photocatalyst which decomposed gradually in air or water. From this study, several MOFs with good photocatalytic activities were synthesized and tested in several degradation processes [168]. Due to their magnificent photocatalytic properties, some MOFs were compared with the most widely used semiconducting materials to date (TiO<sub>2</sub>) [169]. Among these MOFs, Fe-MOFs stand out for their high degradation power as photocatalysts, partly because of their suitable band gap and stability. Compared to MOFs with wide bandgaps, Fe-MOFs are highly attractive. As visible light can directly excite large Fe–O clusters, solar energy can be utilized more efficiently. In addition, they are low-cost and non-toxic catalysts, which make them suitable catalysts for the purification of polluted water [170]. Table 6, shows several examples of modified Fe-MOFs in which the photo-Fenton process has been carried out to degrade a great variety of organic pollutants. The photochemical reactions that occur when iron is used as a transition metal for catalysis are shown below (Equations (17)–(19)) [154]. In the photo-Fenton process, the hydrogen peroxide functions in two ways: by capturing the electrons generated from Fe-MOF (Equation (17)) to produce the hydroxyl radicals (Equation (18)) or by Fenton reaction and to promote the cycling of ≡Fe<sup>3+</sup> to ≡Fe<sup>2+</sup> in the Fe-MOF (Equations (20) and (21)).



Over these years, several limitations were detected such as the same MOFs exhibiting only photocatalytic activity under UV light radiation, poor conductivity or stability. To overcome these limitations, several strategies have been developed by the inclusion of amino groups and the synthesis of Fe-MOFs and heterostructures to utilize the visible light or sunlight. In general, when compared to the parent MOF structures, Fe-MOF composites provide a great improvement in catalytic performance. Thus, by the inclusion of metal oxides such as ZnO nanoparticles to MIL-100-Fe, Ahmad et al. [171] determined that the load of ZnO reduced the electron-hole recombination and enhanced the photodegradation of phenol, bisphenol A and atrazine.

Thus, by the inclusion of metal oxides such as ZnO nanoparticles to MIL-100-Fe, Ahmad et al. [171] determined that the load of ZnO reduced the electron-hole recombination

and enhanced the photodegradation of phenol, bisphenol A and atrazine. An effective photocatalyst was also obtained through the combination of a semiconductor such as  $\text{WO}_3$  with the photosensitive MOF (MIL-53 Fe). It was demonstrated that this material acted as a catalyst for the photo-reduction of Cr(VI) and the photo-oxidation of a known organochlorinated herbicide, 2,4-dichlorophenoxyacetic acid (2,4-D). This indicates that the heterojunction of  $\text{WO}_3$ -MIL-53(Fe) can effectively separate and utilize the pair  $e^-$ - $h^+$  [172]. Another alternative is to consider the MOFs semiconductor-like properties, which promote photogenerated charges to be separated and photocatalytic activities to be enhanced through the hierarchical hybrid by coupling of different MOFs. Thus, MIL-100(Fe) and MIL-53(Fe) with strong visible light absorption were coupled in a hybrid composite (denoted as MIL-100(Fe)@MIL-53(Fe)) by electrostatic attraction at pH 6, due to the fact that MIL-101 was negatively and MIL-53 positively charged [123]. These hybrid MOFs exhibited higher degradation activity and a reduction in the iron released in comparison with single Fe-MOFs.

In recent years, graphite carbon nitride ( $g\text{-C}_3\text{N}_4$ ) has been considered an excellent photocatalytic degrader of pollutants due to its excellent visible light response, stable chemical properties and metal-free properties; however, this material exhibits a low specific surface area. For this reason, in several studies, MOFs have been designed using  $g\text{-C}_3\text{N}_4$  to obtain ideal photocatalysts able to overcome their disadvantages enhancing the photocatalytic surface activity. In the literature, it has been reported that several examples in which co-catalytic synergy between MOFs (ZIF-8, UiO-66, MIL-53, MIL-100, CuBTC, MIL-88B and BUC-21) and  $g\text{-C}_3\text{N}_4$  with different morphologies (sheet, rod and tube) have been tested showing excellent behavior in different degradation processes [173–177].

This kind of heterostructure can provide the following advantages: (i) increased adsorption performance toward targeted models through the development of a large surface area; (ii) accelerated charge transport across the interface and shorter charge transport distances; and (iii) photocatalytically active sites are distributed uniformly. The strong  $\pi$ - $\pi$  interactions of MOFs (with aromatic rings of organic ligands) and  $g\text{-C}_3\text{N}_4$  (triazine rings), together with the abounding surface electrostatic interactions will enable them to achieve close contact, heterojunction construction, and electron transfer effectively [178].

Recently, Pan et al. [179] modified  $g\text{-C}_3\text{N}_4$  by calcination using melamine and cyanuric acid (named CM) based on previous studies, and it was determined that these materials induced stronger optical absorption and increased the lifetime of photoexcited charge compared to unmodified  $g\text{-C}_3\text{N}_4$  [180,181]. Thus, a x% Fe-MOF/CM was prepared with a different mass of MIL-Fe(53) (%) by the self-assembly synthesis method using a co-catalyst CM. It was demonstrated that the best results were obtained when 3% Fe-MOF/CM was selected and the addition of hydrogen peroxide had a synergistic effect enhancing the separation of photogenerated electrons ( $e^-$ ) and holes ( $h^+$ ) effectively. In this variant of Fenton, the photo-Fenton process, using Fe-MOFs and implementing radiation, UV or sunlight, the production of radicals was improved [182] due to  $\equiv\text{Fe}^{3+}$  being constantly reduced (Equation (20)) [183].

As mentioned above, another strategy is the modification of organic linkers in the synthesis of Fe-MOF such as the introduction of an amino group. Thus,  $\text{NH}_2$ -MIL-88B(Fe) or  $\text{NH}_2$ -MIL-101(Fe) exhibited a dual excitation pathway ( $-\text{NH}_2$  and Fe-O center) and was tested with excellent results in the Cr(VI) reduction and the toluene degradation. This kind of photocatalyst could be improved by coupling with  $g\text{-C}_3\text{N}_4$ . Several examples have been reported in the literature, such as  $\text{NH}_2$ -MIL-88B(Fe),  $\text{NH}_2$ -MIL-53(Fe) and  $\text{NH}_2$ -MIL-101(Fe) composites used as photocatalysts to remove several pollutants (Cr (VI) reduction, methylene blue dye, tetracycline, ciprofloxacin, carbamazepine, bisphenol A, p-nitrophenol, ... ) with great efficiency [184–186].

As heterogeneous porous catalysts, these MOFs should adsorb and degrade the target pollutants simultaneously or in series, allowing the operation in a continuous flow without catalyst regeneration. In this sense, Navarathana et al. [169], designed a biochar-MOF hybrid to reduce the particle agglomeration of MIL-53-Fe MOF, increase the mechanical

strength and permit the rapid water flow through fixed beds while dispersing tiny attached MOF particles. For that, the biochar was previously decorated with magnetic  $\text{Fe}_3\text{O}_4$  nanoparticles to create a magnetically manipulable adsorbent. They confirmed that this material was able to adsorb and photodegrade a dye model pollutant such as Rhodamine B. The coexistence of three different adsorbing surface phases allowed a broader application of this unique sorbent.

The separation and recovery of Fe-MOFs from aqueous media present a challenge in wastewater treatment. This limitation may be overcome by immobilizing a powder catalyst on a carrier. By this method, the catalyst could be effectively separated and recovered, and it is also prevented from aggregating, increasing its catalytic efficiency. Wang et al. [187] immobilized MIL-88A(Fe) on cotton fibers (MC) via an in situ method to synthesize MIL-88A(Fe)/MC and evaluated its ability to degrade several antibiotics such as oxytetracycline, tetracycline and chlortetracycline via photoactivated sulfate radical operating in a fixed bed reactor in batch and continuous mode. In this proposed system, peroxydisulfate (PDS) is considered an appealing oxidant. Its activation by MIL-88A(Fe)/MC and UV light irradiation is necessary for sulphate radical generation due to the low reactivity of PDS (Figure 9).

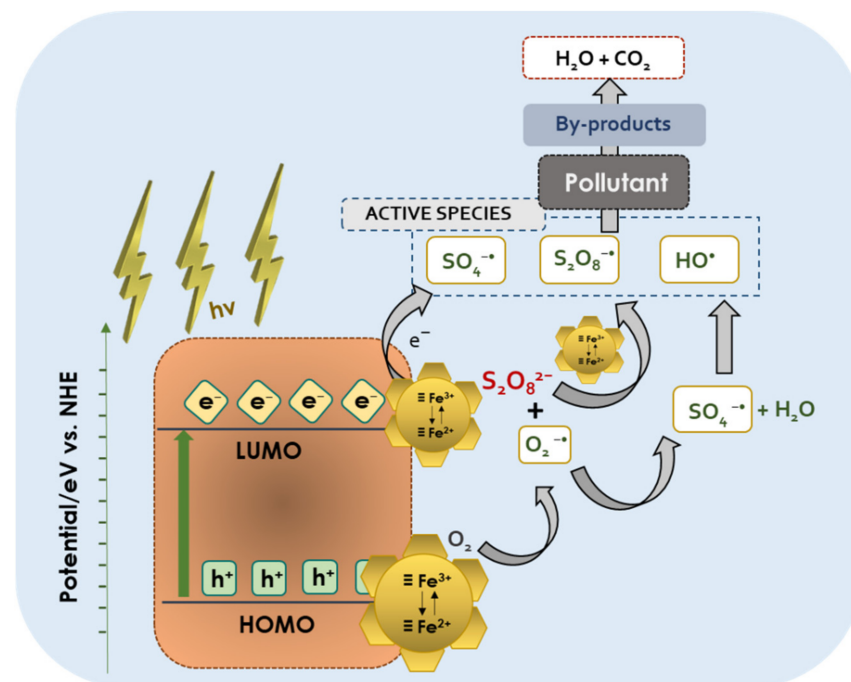
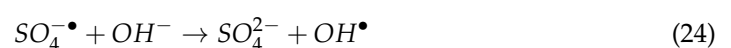
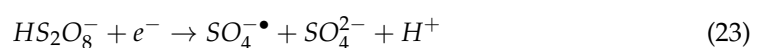


**Figure 9.** Schematic of the proposed mechanism of PDS activation over Fe-MOFs under UV light towards persistent pollutants degradation.

They evaluated the effect of the initial pH on antibiotic degradation efficiency. Thus, at pH values lower than 7 near complete degradation was achieved in 10 min by the sulfate radical generation following Equations (22) and (23). However, at pH values higher than 7, sulfate radicals could be transformed according to Equations (16) and (24), which reduced the concentration of sulphate radicals decreasing the degradation efficiency. In addition, it is important to consider the high stability of MIL-88A(Fe) in acidic conditions [18]. In this context, operation under acidic conditions is favored, so in most cases, it is not necessary to modify the pH of the water to be treated.



In this study, it was demonstrated that MIL-88A(Fe)/MC is extremely stable and reusable by running 30 cycles consecutively, with a well-maintained removal efficiency for each cycle (8 min). These good results were confirmed by the continuous operation of the photoactivated process in a fixed bed reactor with an annular channel and the central cavity was irradiated with a 10 W mercury UV light (UV-Hg) of wavelength 256 nm. Operating at residence times of 10 min, oxytetracycline, tetracycline and chlortetracycline were completely degraded during one day detecting a slight drop in the degradation efficiency at the end hour, showing that one kilogram of MIL-88A(Fe)/MC can treat 23.5 tonnes of polluted water (within a concentration of each antibiotic of 10 mg/L) in one day.

MIL-88AFe was also used to synthesize a photo composite by ball-milling strategy using perylene-34,910-tetracarboxylic diimide (PDINH) [188]. The photocatalyst obtained PDINH/MIL-88A(Fe) was tested in the activation of PDS in the degradation of chloroquine phosphate. The comparison studies with individual compounds (MIL-88A and PDINH) showed a synergic effect with degradation levels around 6 times the level obtained using only photocatalyst pristine MIL-88A(Fe). Thus, this fact could be explained by the synergistic effects from several generated radicals or active species, nonradical singlet oxygen yielded (via directly visible light activation of PDS) and direct and indirect electron transfer activation of PDS over PDINH/MIL-88A(Fe) and MIL-88A(Fe), respectively. This study highlighted that chloroquine phosphate was adsorbed on PDINH/MIL-88A(Fe), reducing the number of active sites and decreasing its degradation efficiency. However, following five re-use cycles, PDINH/MIL-88A(Fe)'s degradation efficiency remained around 94%. Moreover, the physicochemical characterization of the composite confirmed that chloroquine phosphate was adsorbed on PDINH/MIL-88A(Fe) and after five cycles PDINH/MIL-88A(Fe) kept its original structure and morphology, showing good stability and reusability.

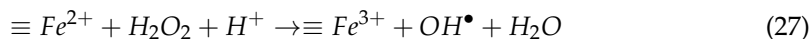
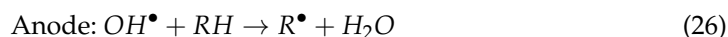
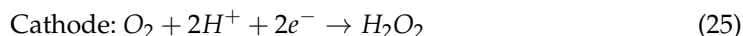
By using a simple solvothermal method, UiO-66 was doped with iron to obtain a solar photocatalyst Fe-UiO-66 and the activation of persulfate under sunlight irradiation to degrade sulfameter in water [189]. This zirconium-based MOF extended the absorption exhibited into sunlight's spectral range by the presence of  $\text{Fe}^{3+}$  when it was doped with iron. As mentioned above, the activation of PS or PMS allowed the recycling of iron due to the presence of the electron donor provided by PS or PMS, allowing the cycling  $\equiv\text{Fe}^{3+}/\equiv\text{Fe}^{2+}$  (Figure 9) in the reaction medium [190]. Thus, the  $\equiv\text{Fe}^{3+}$  detected in Fe-UiO-66 was reduced to  $\equiv\text{Fe}^{2+}$  when PS was added which stimulated the production of sulphate radicals (Equations (15) and (16)). In addition, the presence of iron in the MOF caused a charge transfer from the metal to the cluster and this composite had a large specific surface area that provided more active sites improving the photocatalytic performance. In summary, Lin et al. [189] concluded that the combined reactions produced more free radicals as a result of the photocatalytic and PS processes.

These last studies provided promising approaches for the removal of persistent organic pollutants through the synergistic effects of photocatalysis and PS, PMS or PDS activation over different photocatalysts based on Fe-MOF, with a high sustainability and promising potential of MOFs for continuous wastewater treatment.

#### 4.3. Electrochemical AOP

In this process, the continuous and in situ production of hydroxyl radicals is based on the application of an electric field [191]. To obtain these radicals, a cathode, an anode, a catalyst, which is normally a metal catalyst and an air diffuser, which provides the system with oxygen, are required [192]. These four elements are essential to carry out the organic pollutant mineralization. Therefore, the importance of each of them is explained in the following.

The main function of the cathode is the continuous production of hydrogen peroxide from the reduction of oxygen ( $\text{O}_2$ ) supplied by the air diffuser, as shown in Equation (25) [192]. Thus, once this hydrogen peroxide is produced, the Fenton reaction takes place, which allows the formation of hydroxyl radicals (Equation (27)). Thus, in the anode, the reaction of this radical with the organic pollutant, which is represented in Equation (26) as RH, takes place, and the degraded compound ( $\text{R}\bullet$ ) and water are obtained at the end.



Therefore, catalysts and cathodes are two major factors affecting the reaction rate and efficiency of the electro-Fenton system, so many studies have focused on these two components [193]. Moreover, the main drawback of this process is that  $Fe^{2+}$  is unstable and can cause iron precipitation due to the pH. Therefore, alternative catalysts have been sought to avoid the formation of this precipitate and to avoid affecting the catalysis. Recently, MOFs have attracted attention for their application in electrochemical processes due to their catalytic properties, mechanical stability and good electrical conductivity [194]. Moreover, they are a possible solution to the problem of metal precipitate that occurred because those Fe-MOFs present an interconversion between  $Fe^{3+}$  and  $Fe^{2+}$  and can produce hydroxyl radicals at neutral pH [195].

These Fe-MOFs can also be applied to electrochemical processes using two well-defined strategies: electrocatalyst (by Fe-MOF fixation into the cathode) and application of Fe-MOF in the bulk solution as heterogeneous catalyst.

#### 4.3.1. Electro-Fenton

In the preparation of MOF-based Fe/C cathodes in which the catalyst is immobilized, the main advantage is that, as the catalyst is fixed on the surface (Figure 10a), it is no longer necessary to recover the catalyst from the medium, which is necessary for homogeneous electro-Fenton processes [196]. Thus, carbon felt electrodes were modified by growing MIL-53(Fe) on the surface of a material using a solvothermal synthesis method obtaining a MIL-53(Fe)-based composite material (MIL-53(Fe) @CF) with MOF elongated crystals uniformly distributed on the carbon felt (CF) [197]. Using MIL-53(Fe) instead of another iron salt, minimal leaching of iron into solutions was detected and the possibility was opened up to operate at natural water pH of around 7. In addition, agglomerates or nanoparticles of iron oxide were not detected after treatment. The obtained good results were ascribed to the large accessible pore volume and higher accessible surface area that favor the  $H_2O_2$  production and the surface catalyzed reactions.

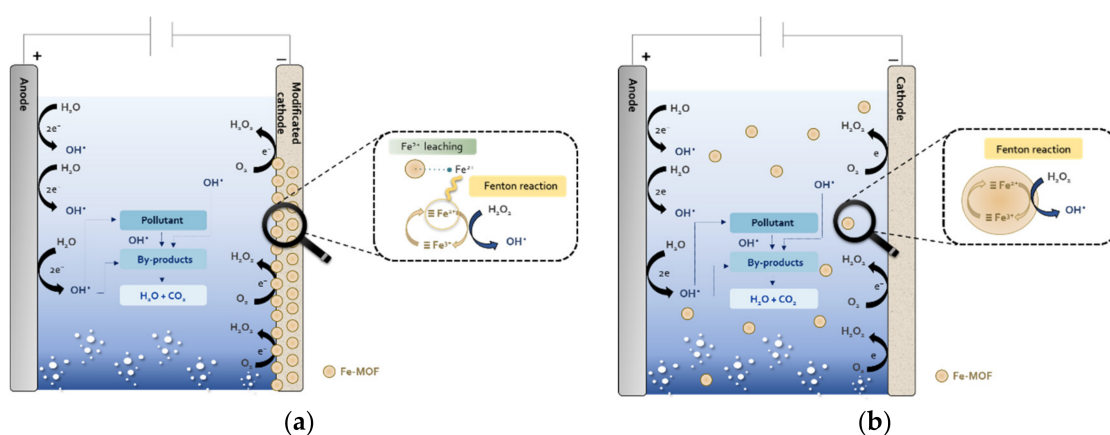


**Figure 10.** General scheme of the degradation electro-Fenton processes using (a) modified cathode with Fe-MOF and (b) Fe-MOF in bulk solution.

An important challenge in heterogeneous catalysis is the agglomeration of catalysts. To overcome this limitation, recent studies have shown that catalysts with a transition metal nanoparticle core and a graphitized porous carbon shell have remarkably enhanced catalytic activity and stability [196]. In this sense, electro-Fenton processes exhibit excellent performance with MOF-derived micro-/nano-materials as MOF-derived core-shell structured materials.

Several examples have been reported in the literature in which novel catalysts were constructed from Fe-MIL. Thus, Tang and Wang designed a magnetic Fe@mesoporous carbon (Fe@MesoC) and flower-like FeCu@C derived from MIL-100(Fe) and (Fe, Cu)-BDC, respectively, that presented a dual reaction site as highly reactive Fenton catalysts for efficient removal of pollutants as sulfanilamide antibiotics [198]. Similarly, Du et al. designed the synthesis of an S-modified MIL-53 (Fe) catalyst by a sulfurizing process [199] determining the positive effect of S in the catalyst enables quick pH adjustments and promotes the generation of  $\text{Fe}^{2+}$ , which, in turn, efficiently activates  $\text{H}_2\text{O}_2$  to form  $\text{OH}^-$ .

Liu et al. [200] followed the strategy of adding a carbonized Fe-MOF (CMOF) in porous carbon monoliths (PCM), so it was named CMOF@PCM. Furthermore, their results showed that the MOF precursor to obtaining the CMOF@PCM influenced the final structure of the CMOF@PCM and the catalysis activity to carry out the electro-Fenton process. They synthesized and used several Fe-MOFs (MIL-88(Fe), MIL-100(Fe) and MIL-101(Fe)) to study the influence of the MOF precursor and the functionalization of Fe-MOFs (MIL-88(Fe)- $\text{NH}_2$  and MIL-101(Fe)- $\text{NH}_2$ ). From the electrochemical performance study, they were able to determine that the efficiency decreased in the  $\text{CMIL-100(Fe)@PCM} > \text{CMIL-88(Fe)@PCM} > \text{CMIL-101(Fe)@PCM}$ . Regarding the influence of the functional groups, it was confirmed that the use of amine-functionalized  $\text{CMIL-88(Fe)-NH}_2\text{@PCM}$  improved the removal of the pollutant (73.42%) while with the corresponding  $\text{CMIL-101(Fe)-NH}_2\text{@PCM}$ , this catalytic capacity worsened (53.63%). So, there was no conclusion about the influence of the functional groups on Fe-MOFs. After analyzing these two effects, they selected  $\text{CMIL-100@PCM}$  as the ideal. Additionally, to examine how the amount of PCM influence the process and pollutant degradation, several MOFs were synthesized in a range of 10–75 wt%. The first thing to note is that the PCM favored the process in comparison to the control process without PCM in which the maximum degradation was only 11.8%. Regarding the amount of PCM to be used, it was observed that when the PCM increased the percentage of elimination improved until a maximum when the amount was 25% PCM. Therefore, they concluded that the  $\text{CMIL-100@PCM}_{25}$  catalyst was the best because it could remove near complete the herbicide pollutant, napromide, in 1 h. Moreover, it could be used in three cycles practically without altering its herbicide removal capacity.

Within this strategy, Fu et al. [201] were able to fabricate a modified graphite (GF) electrode using a bimetallic MOF as a precursor, named  $\text{Cu}_{0.33}\text{Fe}_{0.67}\text{NBDC-300/GF}$  to degrade SMX. The main improvement achieved by synthesizing this electrode was that the regeneration of  $\text{Fe}^{2+}$  was considerably accelerated due to the coexistence of the  $\text{Fe}^{2+}/\text{Fe}^{3+}$  and  $\text{Cu}^+/\text{Cu}^{2+}$  redox reactions. In addition, another improvement incorporated in the electro-Fenton process was that it favored the generation of more active radicals, such as  $\text{OH}^\bullet$  (Equation (11)) and  $\text{O}_2^{\bullet-}$  (Equation (10)). These two radicals were suggested because, during the study of the generation of the radicals, they detected that up to 45 min the degradation of SMX was due to the free  $\text{OH}^\bullet$  and the ones bound to the electrode surface. However, from 45 to 75 min,  $\text{O}_2^{\bullet-}$  was found to play an important role in the degradation. In fact, at 75 min, SMX was completely eliminated in a pH range of 4 to 9. As well as allowing it to operate in a wide pH range, it has high stability and can be used in several reuses; in this case, five cycles were made, without affecting its catalytic activity.

The second strategy employed is the addition of suspended heterogeneous catalysts in the bulk solutions, as illustrated in Figure 10b.

For this strategy, we can highlight the study performed by Ye et al. [202], in which a MOF-engineered  $\text{FeS}_2/\text{C}$  nanocomposite was synthesized. This catalyst was fabricated from a Fe-MOF precursor which they added sulfur and subjected it to carbonization and sulfidation, simultaneously. By operating in this mode, they produced well-dispersed  $\text{FeS}_2$  pyrite nanoparticles, approximately 100 nm in diameter, bound to porous carbon. The reason for this synthesis was to solve the problem presented by pyrite, which, despite being an excellent donor and a catalyst with an outstanding performance in electro-Fenton processes, is not used due to its high iron leaching. Therefore, this  $\text{FeS}_2$  nanocatalyst is intended to solve this problem and has similar properties that characterize pyrite. To study

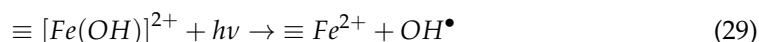
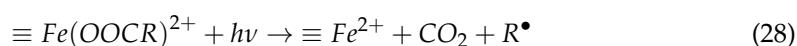
the catalytic capacity of the FeS<sub>2</sub>/C nanocatalyst in the electro-Fenton process, an anode of boron-doped diamond (BDD) was used and as a cathode, carbon cloth coated with carbon-polytetrafluoroethylene (PTFE), which is a type of electrode commercially available from BASF. Using this configuration, the system was optimized and it was established that the optimal operating conditions were a pH close to neutral, a current intensity of 50 mA and a catalyst load of 0.4 g/L, achieving a fluoxetine removal level of around 92% after 1 h. In addition, its reusability was also demonstrated. Based on this study, it was found that the catalyst retains its catalytic properties even after being reused five cycles; however, its catalytic properties were reduced as the number of cycles increased. In the fifth cycle, only 61% could be eliminated. Therefore, with the MOF-engineered FeS<sub>2</sub>/C nanocatalyst, it was possible to have the FeS<sub>2</sub> on the surface of the carbon and to solve the problem of pyrite reusability in the electro-Fenton process. Due to the possible self-decomposition of Fe-MOF in water, these authors also developed a heterogeneous electro-Fenton process using as catalyst magnetic MIL(Fe)-type MOF-derived N-doped nano-ZVI@C rods synthesized by pyrolysis of MIL-88B and NH<sub>2</sub>-MIL(Fe)-88 in an inert atmosphere at 800 °C [203]. This final step induced the carbonization of organic polymers, resulting in highly porous carbon with magnetic properties transforming the metal MOF into magnetic nanosized MOF. The high porosity of this material minimizes the limitations of mass transport and its ferromagnetic characteristic improves the catalyst recovery process at the end of the process. In comparison with MIL-88B and NH<sub>2</sub>-MIL(Fe)-88 at natural pH 5.5, nano-ZVI@C obtained from NH<sub>2</sub>-MIL(Fe)-88 with a total abatement after 1 h, this catalyst demonstrated its superiority. It was determined that the ferric/ferrous iron took place on the catalyst surface and the presence of amino group improves the degradation process due the decreasing the carbon bandgap energy.

Following this line, recently Du et al. [204] obtained an efficient bimetallic catalyst Fe-Mo by calcination MIL-53(Fe)@MoO<sub>3</sub> (FeMo@PC). In this bimetallic material is highlighted the electron transfer between them and the possibility of continuous regeneration on the cathode increases the hydrogen peroxide decomposition. Thus, using this bimetallic catalyst, the effect of Mo co-catalysis was confirmed, in which ≡Mo<sup>4+</sup> reduced ≡Fe<sup>3+</sup> to ≡Fe<sup>2+</sup> that could follow the Fenton reaction. It is outstanding the high degradation level achieved for several persistent pollutants (SMT, phenol, 2,4-dichlorophenoxyacetic acid and CBZ) with a catalyst load of 25 mg/L and current intensity of 5 mA.

Based on the excellent results of electro-Fenton and photo-based AOPs the development of the photo-electro-Fenton process is an upgraded electro-Fenton process.

#### 4.3.2. Photoelectro-Fenton

This process is a combination of electro-Fenton with radiation (UV or sunlight) and allows to achieve higher production of the hydroxyl radical (Figure 11) [195]. Based on the literature is was confirmed that the UV photons can reduce the ≡Fe<sup>3+</sup>, either complexed with a carboxylated organic (R-COO<sup>-</sup>) via reaction (Equation (28)) or in its hydrated form via photo-Fenton reaction (Equation (29)), thus promoting the continuous ≡Fe<sup>2+</sup> regeneration.



To improve this hybrid process, it is important the selection of a good photoelectric catalysis performance since it determines the additional generation of these radicals [205]. A Fe-O cluster, which is photosensitive, is also an advantage of Fe-MOFs in the photo-electro-Fenton process, as discussed in Section 4.2.

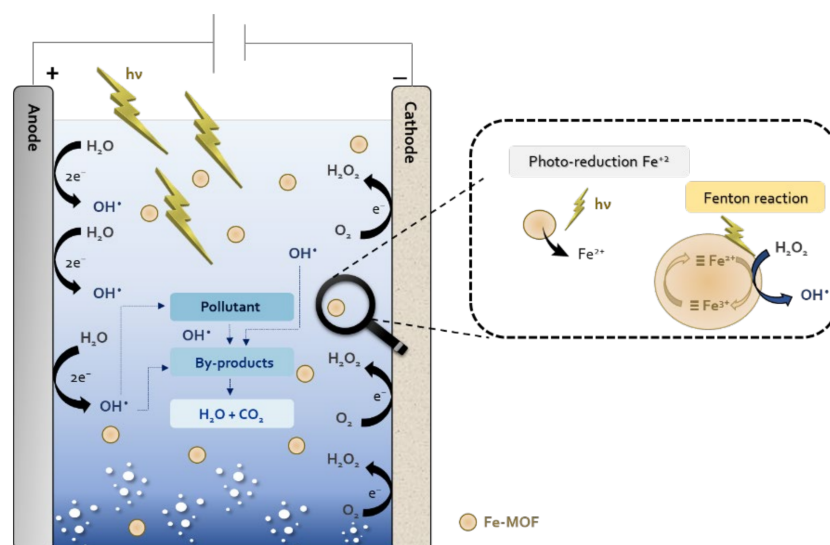


**Figure 11.** Schematic representation of the photo-electro-Fenton process with Fe-MOF as suspended heterogeneous catalysts.

The studies of Qi et al. [205] and Du et al. [206] should be emphasized due to their incorporation of new bimetallic Fe-MOFs within the photo-electro-Fenton processes. Regarding the study of Qi et al. [205], MOF-525-Fe/Zr is synthesized and with this MOF the CF is coated to fabricate the modified cathode, which is called MOF-525-Fe/Zr@CF. When carrying out the characterization study of this material, the main difference between MOF-525 and MOF-525-Fe/Zr is the large increase in pore area and pore volume. In fact, in this study, it was found that most of the pores of both MOFs are mesoporous and over a diameter of 2–10 nm. In this study, these authors evaluated the catalytic capacity of this new material in comparison to four other materials such as CF, MOF-525@CF (which is the pure MOF-525), Fe-MOF-525@CF and Fe<sub>3</sub>O<sub>4</sub>@MOF-525@CF, to check the improvement that the MOF-525-Fe/Zr provides. From this study, it could be concluded that there is an influence on the catalyst preparation as the post-modified Fe-MOF-525@CF showed no significant difference in degradation performance from pure MOF-525 and common CF, both having degradation rates below 50%. As for the Fe<sub>3</sub>O<sub>4</sub>@MOF-525@CF, it showed a slightly worse SMX removal rate (70%) than the MOF-525-Fe/Zr (97.3%). This is due to the Fe<sub>3</sub>O<sub>4</sub>@MOF-525@CF being a post-assembly synthesis, as it can only control MOF growth and failed to achieve further charge transfer beyond the interfacial energy barrier. A drawback of this cathode is that its performance depends on the environmental conditions to which it is subjected as it can only work at pH below 4, with an optimum pH of 3. The main reason for this considerable reduction is that the carboxylic acid groups, which are the connectors between Zr-oxo SBUs and Fe-TCPP, can be partially polarized. Despite this drawback, this modified cathode showed promising results in SMX removal in different wastewaters (tap water and river water) and improves the mineralization rate (85% total organic carbon (TOC) mineralization rate) compared to other works using MOFs such as Hang et al. [207], which using a photo-Fenton process manages to completely remove SMX in 40 min but its mineralization rate is 41%.

Similarly, Du et al. [206] synthesized a bimetallic catalyst, called FeCu@porous carbon (PC). This catalyst was derived from Fe/Cu-MOFs through the pyrolysis process. In order to check the efficiency of the catalyst in the photo-electro-Fenton process, a comparison with the electro-Fenton process and photocatalysis was made to remove SMT. From this study, it was concluded that the FeCu@PC/photo-electro-Fenton system presented the highest removal efficiency after 30 min (96.4%) compared to the FeCu@PC/electro-Fenton (79.3%) and FeCu@PC/UV (30.8%) systems. This improvement in efficiency may be due to the good photoelectric synergy and also to its high production of the hydroxyl radicals, which reached a concentration of 162.1  $\mu\text{mol/L}$  after 1 h, which is approximately twice as high as

in the electro-Fenton process. Another point in favor of the FeCu@PC/photo-electro-Fenton system is that leaching of the Fe (1.18 mg/L) and Cu (0.67 mg/L) metals are slightly lower than in the FeCu@PC/electro-Fenton system (1.38 mg/L and 0.91 mg/L, respectively). However, they also tested the catalyst stability in both systems. Surprisingly, the SMX removal capacity of the catalyst in the photo-electro-Fenton system is not practically affected while in the other one, the drop is very pronounced. In fact, this behavior was clearly observed when compared to the removal rates between the first cycle, which was around 90%, and the second, which was around 60%. This shows that the catalyst is not suitable for the FeCu@PC/electro-Fenton system in the flow system because the catalyst lost its properties with the use.

Another relevant aspect of this catalyst is its versatility since the FeCu@PC/photo-electro-Fenton system is also able to successfully degrade other pollutants, such as phenol (99.1%), CBZ (99.7%) and 2,4-D (99.9%). In addition, this catalyst has accelerated the mineralization process by removing more than 60% of each of the pollutants within 1 h: SMT (73.3%), phenol (65.3%), CBZ (72.2%) and 2,4-D (79.4%).

Therefore, little by little, Fe-MOFs are being incorporated in wastewater treatment by means of electrochemical AOPs and are proving to have high efficiency in the elimination of these organic pollutants and stability, which allows them to be used on several occasions and become a viable catalyst for the circular economy and the sustainability of the process.

#### 4.4. Ozone-Based AOP

Ozonation allows the oxidation of organic pollutants in water through the use of ozone, allowing the generation of the hydroxyl radical [208,209]. In addition, this process, as shown in Figure 6, can also be combined with other oxidants and examples of this combination can be ozone with hydrogen peroxide or ultraviolet radiation [208]. As with the previous processes explained above, metal ions (Ni, Cu, Fe or Mn) and metal oxides (copper oxide, manganese dioxide, titanium dioxide or iron oxide) can be used to accelerate the degradation reaction [210]. At present, the mechanisms of this process are complex and complicated to understand [211]. However, it can be assumed that the following chemical reaction (Equation (30)) occurs that allows the generation of the hydroxyl radicals by using a transition metal catalyst [212].



A drawback of this type of AOP is that ozone has a short half-life and this means that the costs associated with full-scale water treatment of these processes are expensive. Furthermore, regarding the use of Fe-MOF in ozone-based AOPs, few papers have been reported between 2018 and 2022. However, the use of MOFs as a catalyst can overcome its limitations.

Among the studies reported in the literature, the study of Mohebbi et al. [213] in which Fe<sub>3</sub>O<sub>4</sub>@Ce-UiO-66 was synthesized by the combination of Fe<sub>3</sub>O<sub>4</sub> nanoparticles with the MOF, Ce-UiO-66 is highlighted. This catalyst system showed a rapid and total elimination of acetaminophen in only 10 min. Furthermore, this catalyst has high catalytic efficiency in successive cycles with a loss of activity of less than 10% on the acetaminophen degradation, making it a promising catalyst. Chen et al. [214] used Co<sub>3</sub>O<sub>4</sub>-C@FeOOH, which is a derivative of ZIF-67, as a catalyst to remove the drug norfloxacin, showing an excellent catalyst activity for the ozonation process achieving the complete degradation after 7 min, keeping this good activity during several cycles of use. Yu et al. [215] evaluated the heterogeneous ozonation using MOF MIL-88A(Fe) to eliminate a phenolic compound, 4-nitrophenol. The results of this process were also promising with degradation levels higher than 90% in 30 min. It is outstanding that the elimination of this compound remains practically the same after four consecutive cycles, which is indicative of the high stability of this catalyst.

In summary, although few studies have used Fe-based MOFs as ozonation catalysts, their use makes this heterogeneous process a very promising technology.

**Table 6.** Summary of some of the Fe-MOF in catalyst, photocatalyst and electrochemical AOPs.

MOF	Pollutants	AOP	Removal (%Degradation/Time (min))	Reuses (n° Cycles/% Degradation)	Reference
3 % Fe-MOF/CM	TC	Photocatalytic/H <sub>2</sub> O <sub>2</sub>	100%/60 min	4/90%	[179]
g-C <sub>3</sub> N <sub>4</sub> /NH <sub>2</sub> -MIL-101(Fe)	Acetaminophen	Photocatalytic/H <sub>2</sub> O <sub>2</sub>	94%/60 min	10/>85%	[216]
g-C <sub>3</sub> N <sub>4</sub> /PDI@NH <sub>2</sub> -MIL-53(Fe)	TC	Photocatalytic/H <sub>2</sub> O <sub>2</sub>	90%/60 min	5/-	[185]
g-C <sub>3</sub> N <sub>4</sub> /PDI@NH <sub>2</sub> -MIL-53(Fe)	Carbamazepine (CBZ)	Photocatalytic/H <sub>2</sub> O <sub>2</sub>	75%/150 min	5/-	[185]
g-C <sub>3</sub> N <sub>4</sub> /PDI@NH <sub>2</sub> -MIL-53(Fe)	BPA	Photocatalytic/H <sub>2</sub> O <sub>2</sub>	100%/10 min	5/-	[185]
g-C <sub>3</sub> N <sub>4</sub> /PDI@NH <sub>2</sub> -MIL-53(Fe)	4-NP	Photocatalytic/H <sub>2</sub> O <sub>2</sub>	100%/30 min	5/-	[185]
MIL-88A(Fe)/MC	Oxytetracycline (OTC)	Photoactivated sulfate radical	98.2%/240 min	30/83.7%	[187]
MIL-88A(Fe)/MC	TC	Photoactivated sulfate radical	98.3%/240 min	30/78.8%	[187]
MIL-88A(Fe)/MC	Chlortetracycline (CTC)	Photoactivated sulfate radical	100%/240 min	30/88.1%	[187]
6%MIL-88A@BCN	Phenol	Photocatalytic/H <sub>2</sub> O <sub>2</sub>	92.7%/30 min	5/93–88%	[217]
6%MIL-88A@RCN	Phenol	Photocatalytic/H <sub>2</sub> O <sub>2</sub>	91.1%/30 min	5/92–87%	[217]
Bi <sub>5</sub> O <sub>7</sub> I@MIL-100(Fe)	Doxycycline	Photoactivated sulfate radical	100%/130 min	5/100–90%	[218]
BiOBr/MIL-53(Fe)	CBZ	Photocatalytic/H <sub>2</sub> O <sub>2</sub>	85%/100 min	0	[219]
Fe <sub>3</sub> O <sub>4</sub> @MIL-53(Fe)	Ibuprofen	Photocatalytic/H <sub>2</sub> O <sub>2</sub>	99%/60 min	5/95%	[220]
Fe-UiO-66	Sulfameter	Photoactivated sulfate radical	90%/300 min	5/99–95%	[189]
MIL-101(Fe)/TiO <sub>2</sub>	TC	Photocatalytic/H <sub>2</sub> O <sub>2</sub>	92.8%/10 min	5/93–90%	[221]
PDINH/MIL-88A	Chloroquine phosphate	Photoactivated sulfate radical	94.6%/30 min	5/93.8%	[188]
AFG@30MIL-101(Fe)	Diazinon	Photo-Fenton	100%/105 min	4/100–97%	[222]
AFG@30MIL-101(Fe)	Atrazine	Photo-Fenton	81%/105 min	4/81–75%	[222]
Cu <sub>2</sub> O/MIL(Fe/Cu)	Thiacloprid	Photo-Fenton	82.3%/80 min	10/>95%	[223]
Co-Fe PBAs	Levofloxacin	Fenton-like with PMS	97.6%/30 min	5/83.7%	[164]
CUMSs/MIL-101(Fe,Cu)	Hydrochloride CIP	Fenton-like	93.5%/30 min	4/88.4%	[224]
Fe(PyBDC)	SMX (Sulfamethoxazole)	Fenton-like with PS	98.7%/180 min.	2/0%, it can not be reused	[163]
Basolite F-300	Antipyrine	Fenton-like with PMS	100%/300 min	4/93%	[225]
Basolite F-300	<i>Escherichia coli</i>	Fenton-like with PMS	100%/5 min	4/100%	[225]
Fe@MesoC	SMX	Fenton	100%/120 min	3/85.2%	[160]
Fe <sub>0.75</sub> Cu <sub>0.25</sub> (BDC)	SMX	Fenton-like	100%/120 min	3/99–98%	[161]
Fe <sub>3</sub> O <sub>4</sub> @MIL-100(Fe)	Levofloxacin	Photo-Fenton	93.4%/180 min	5/>80%	[224]
Fe <sup>II</sup> -MIL-53(Fe)	4-NP	Fenton-like	95.2%/120 min	5/89%	[227]
Fe-BDC-NH <sub>2</sub>	Bisphenol A (BPA)	Fenton-like	95%/10 min	5/>90%	[162]
Fe-ISAs@CN	Sulfadiazine (SDZ)	Fenton-like	96%/60 min	5/>70%	[228]
Fe-Pd@C nanomaterial	Phenol	Fenton	95%/60 min	5/75%	[136]
Fe-TCPP-3	CIP	Photo-Fenton	73%/30 min	0	[229]
M.MIL-100(Fe)@ZnO NS	Phenol, BPA and atrazine	Photo-Fenton	92%/120 min (mean value of all pollutants)	5/>85% (mean value of all pollutants)	[171]
MIL-100(Fe)-M (H <sub>3</sub> BTC/4 NaOH)	Sodium sulfadiazine	Photo-Fenton	95%/240 min	5/95–90%	[230]
MIL-101(Fe)-NH <sub>2</sub> @Al <sub>2</sub> O <sub>3</sub> (MA)	Norfloxacin	Photo-Fenton	97.3%/100 min	10/97%	[231]
MIL-53(Fe)@PES	CBZ	Photo-Fenton	99%/60 min	5/80%	[232]
r-MIL-88A-Fe	Phenol	Fenton	100%/15 min	3/97%	[158]
Ti <sub>3</sub> C <sub>2</sub> T <sub>x</sub> /MIL-53(Fe) hybrid	TC	Photo-Fenton	90%/80 min	5/85%	[233]
VC@Fe <sub>3</sub> O <sub>4</sub> nanoparticles	SDZ	Fenton-like	56.6%/90 min	3/26.2%	[234]
CMIL-100(Fe)@PCM25	Napropamide	Electro-Fenton	97%/60 min	3/95–85%	[200]
Cu <sub>0.33</sub> Fe <sub>0.67</sub> NBDC-300/GF	SMX	Electro-Fenton	100%/75 min	5/95%	[201]
Fe bpydc	Bezafibrate	Photo-electro-Fenton	96%/90 min	3/67%	[195]
Fe/Fe <sub>3</sub> C@PC	SMT	Electro-Fenton	99.2%/60 min	2/57%	[196]
FeCu@PC	SMT	Photo-electro-Fenton	99.9%/60 min	5/97%	[206]
MOF-525-Fe/Zr@CF	SMX	Photo-electro-Fenton	97.3%/180 min	4/96.6%	[205]
FeS <sub>2</sub> /C	Fluoxetine	Electro-Fenton	91%/60 min	5/61%	[202]
Mn/Fe@PC	Triclosan	Electro-Fenton	100%/120 min	6/99%	[235]
Fe <sup>2+</sup> /NDCA	Dimethyl phthalate	Electro-Fenton	100%/50 min	5/95–90%	[236]
Fe <sup>2+</sup> /NDCA	3-Chlorophenol	Electro-Fenton	100%/30 min	0	[236]
Fe <sup>2+</sup> /NDCA	BPA	Electro-Fenton	100%/10 min	0	[236]
Fe <sup>2+</sup> /NDCA	SMX	Electro-Fenton	100%/15 min	0	[236]
NH <sub>2</sub> -MIL(Fe)-88B (nano-ZVI@C-N)	Gemfibrozil	Electro-Fenton	95%/60 min	5/80–75%	[203]

## 5. Conclusions

This study has provided a review of the recent progress in the research and practical application of MOFs, mainly Fe-MOFs, with a special emphasis on their potential as catalysts in heterogeneous AOPs. Thus, it has been also shown that Fe-MOF structures can be rationally designed through several synthesis methods and details about these procedures are summarized in Table 4. Based on the extensive literature reviewed, it is also concluded that this great designability of Fe-MOFs allows obtaining catalysts on-demand,

able to improve the removal of persistent pollutants from wastewater by means of the selected AOPs, as summarized in Tables 5 and 6. Lastly, the synthesis of Fe-MOFs by doping with other metals or adding several agents provides an effective way to accelerate the redox cycle of  $\text{Fe}^{3+}/\text{Fe}^{2+}$  and promote the radical generation and/or increase the selectivity of the catalysts by the removals of the pollutants present in the wastewater.

However, although more than one thousand studies have been published in the last five years about this topic, there is still a long way to go for Fe-MOFs to be consolidated as catalysts and to be viable for large-scale use. Compiling this collection of studies, it is possible to say that this future is not very far away. The prospect of their usage for Fe-MOF based AOPs presents several aspects and future opportunities related to the removal of emerging pollutants:

- Eco-friendly preparation of MOFs: search for alternative methods for MOF synthesis with high yield and using environmentally friendly and harmless solvents.
- Bimetallic MOFs: application of various transition metals in the synthesis of the MOF enhancing their properties for the AOPs;
- New composite materials hybridized with MOFs: exploration of new materials to be introduced on MOFs adding new functions and achieving high-performance of the catalyst.
- Shelf life and reusability: these are prerequisites for long-term industrial use. The improvement of the stability of MOFs for their use in aqueous environments is required because most of them are unstable in water and decompose. Moreover, their recovery and reuse in several cycles or continuous treatment is a crucial factor in the scale-up of the processes.
- Emerging contaminants treatment and real wastewater use: mostly dye degradation is studied using MOF, but emerging contaminants are barely studied, and it is required to give more attention to these compounds in the future. Another consideration is the evaluation of real wastewater in the treatments due to most of the actual ones are performed using simulated ones.

**Author Contributions:** Conceptualization, M.P., E.R. and A.S.; resources, A.F.-S. and A.S.; writing—original draft preparation, A.F.-S.; writing—review and editing, A.F.-S., A.S. and E.R.; visualization, A.F.-S., M.P., E.R. and A.S.; supervision, M.P., E.R. and A.S.; project administration, M.P. and A.S.; funding acquisition, M.P. and A.S. All authors have read and agreed to the published version of the manuscript.

**Funding:** This research has been financially supported by Project PID2020-113667GB-I00, funded by MCIN/AEI/10.13039/501100011033 and Xunta de Galicia, and the European Regional Development Fund (ED431C 2021-43).

**Institutional Review Board Statement:** Not applicable.

**Informed Consent Statement:** Not applicable.

**Data Availability Statement:** Not applicable.

**Acknowledgments:** Antía Fdez-Sanromán thanks Universidade de Vigo and Ministerio de Ciencia e Innovación (PRE2021-098540) for her predoctoral fellowships.

**Conflicts of Interest:** The authors declare no conflict of interest.

## References

1. Sales, H.B.; Menezes, R.R.; Neves, G.A.; de Souza, J.J.N.; Ferreira, J.M.; Chantelle, L.; de Oliveira, A.L.M.; Lira, H.d.L. Development of Sustainable Heterogeneous Catalysts for the Photocatalytic Treatment of Effluents. *Sustainability* **2020**, *12*, 7393. [[CrossRef](#)]
2. Natarajan, S.; Bajaj, H.C.; Tayade, R.J. Recent Advances Based on the Synergetic Effect of Adsorption for Removal of Dyes from Waste Water Using Photocatalytic Process. *J. Environ. Sci.* **2018**, *65*, 201–222. [[CrossRef](#)] [[PubMed](#)]
3. Cheng, M.; Lai, C.; Liu, Y.; Zeng, G.; Huang, D.; Zhang, C.; Qin, L.; Hu, L.; Zhou, C.; Xiong, W. Metal-Organic Frameworks for Highly Efficient Heterogeneous Fenton-like Catalysis. *Coord. Chem. Rev.* **2018**, *368*, 80–92. [[CrossRef](#)]
4. Dhaka, S.; Kumar, R.; Deep, A.; Kurade, M.B.; Ji, S.W.; Jeon, B.H. Metal-Organic Frameworks (MOFs) for the Removal of Emerging Contaminants from Aquatic Environments. *Coord. Chem. Rev.* **2019**, *380*, 330–352. [[CrossRef](#)]

5. Wang, J.; Wang, S. Reactive Species in Advanced Oxidation Processes: Formation, Identification and Reaction Mechanism. *Chem. Eng. J.* **2020**, *401*, 126158. [CrossRef]
6. De Rosa, S.; Giordano, G.; Granato, T.; Katovic, A.; Siciliano, A.; Tripicchio, F. Chemical Pretreatment of Olive Oil Mill Wastewater Using a Metal–Organic Framework Catalyst. *J. Agric. Food Chem.* **2005**, *53*, 8306–8309. [CrossRef]
7. Zorainy, M.Y.; Sheashea, M.; Kaliaguine, S.; Gobara, M.; Bo, D.C. Facile Solvothermal Synthesis of a MIL-47 (V) Metal–Organic Framework for a High-Performance Epoxy/MOF Coating with Improved Anticorrosion Properties. *RSC Adv.* **2022**, *12*, 9008–9022. [CrossRef]
8. Pasandideh, Y.; Razmi, H. Introduction of a Zn-Based Metal–Organic Framework @ Biomass Porous Activated Carbon as a High-Sensitive Coating for a Stainless Steel SPME Fiber: Application to the Simultaneous Analysis of Nonsteroidal Anti-Inflammatory Drugs. *BMC Chem.* **2022**, *16*, 25. [CrossRef]
9. El Taher, B.J.; Sabouni, R.; Ghommem, M. Luminescent Metal Organic Framework for Selective Detection of Mercury in Aqueous Media: Microwave-Based Synthesis and Evaluation. *Colloids Surf. A Physicochem. Eng. Asp.* **2020**, *607*, 125477. [CrossRef]
10. Zhong, Q.; Xu, C.; Liu, Y.; Ji, Q.; Xu, Z.; Sun, D.; Zhou, S.; Yang, B.; Dai, Y.; Qi, C.; et al. Defect-Engineered FeSe<sub>2</sub>-x@C with Porous Architecture for Enhanced Peroxymonosulfate-Based Advanced Oxidation Processes. *Appl. Catal. B Environ.* **2022**, *309*, 121259. [CrossRef]
11. Kampoouraki, Z.C.; Giannakoudakis, D.A.; Nair, V.; Hosseini-Bandegharai, A.; Colmenares, J.C.; Deliyanni, E.A. Metal Organic Frameworks as Desulfurization Adsorbents of DBT and 4,6-DMDBT from Fuels. *Molecules* **2019**, *24*, 4525. [CrossRef]
12. Pi, Y.; Li, X.; Xia, Q.; Wu, J.; Li, Y.; Xiao, J.; Li, Z. Adsorptive and Photocatalytic Removal of Persistent Organic Pollutants (POPs) in Water by Metal–Organic Frameworks (MOFs). *Chem. Eng. J.* **2018**, *337*, 351–371. [CrossRef]
13. Hou, J.; Wan, J.; Yan, Z.; Wang, Y.; Ma, Y.; Xie, Y.; Chen, H.; Xue, Y. A Novel Polydopamine-Modified Metal Organic Frameworks Catalyst with Enhanced Catalytic Performance for Efficient Degradation of Sulfamethoxazole in Wastewater. *Chemosphere* **2022**, *297*, 134100. [CrossRef]
14. Li, J.; Zhu, W.; Gao, Y.; Lin, P.; Liu, J.; Zhang, J.; Huang, T. The Catalyst Derived from the Sulfurized Co-Doped Metal–Organic Framework (MOF) for Peroxymonosulfate (PMS) Activation and Its Application to Pollutant Removal. *Sep. Purif. Technol.* **2022**, *285*, 120362. [CrossRef]
15. Singh, S.; Numan, A.; Cinti, S. Point-of-Care for Evaluating Antimicrobial Resistance through the Adoption of Functional Materials. *Anal. Chem.* **2022**, *94*, 26–40. [CrossRef]
16. Zhao, F.; Fang, S.; Gao, Y.; Bi, J. Removal of Aqueous Pharmaceuticals by Magnetically Functionalized Zr-MOFs: Adsorption Kinetics, Isotherms, and Regeneration. *J. Colloid Interface Sci.* **2022**, *615*, 876–886. [CrossRef]
17. Yadav, A.; Bagotia, N.; Sharma, A.K.; Kumar, S. Advances in Decontamination of Wastewater Using Biomass-Based composites: A Critical Review. *Sci. Total Environ.* **2021**, *784*, 147108. [CrossRef]
18. Yuan, S.; Feng, L.; Wang, K.; Pang, J.; Bosch, M.; Lollar, C.; Sun, Y.; Qin, J.; Yang, X.; Zhang, P.; et al. Stable Metal–Organic Frameworks: Design, Synthesis, and Applications. *Adv. Mater.* **2018**, *30*, 1704303. [CrossRef]
19. The Cambridge Crystallographic Data Center (CCDC) CSD MOF Collection. Available online: <https://www.ccdc.cam.ac.uk/Community/csd-community/csd-mof-collection/> (accessed on 8 November 2021).
20. Li, Y.; Jing, X.; Li, Q.; Shen, Y.; Fang, Q. Well-Defined Bimetal Oxides Derived from Prussian Blue Analogues with Regulable Active Sites for Phosphate Removal. *J. Colloid Interface Sci.* **2022**, *622*, 390–401. [CrossRef]
21. Hariri, R.; Dehghanpour, S. Adsorptive Removal and Visible-Light Photocatalytic Degradation of Large Cationic and Anionic Dyes Induced by Air-Bubbles in the Presence of a Magnetic Porphyrinic Metal–Organic Framework (Fe<sub>3</sub>O<sub>4</sub>@SiO<sub>2</sub>@PCN-222(Fe)). *J. Phys. Chem. Solids* **2021**, *155*, 110126. [CrossRef]
22. Kirchon, A.; Zhang, P.; Li, J.; Joseph, E.A.; Chen, W.; Zhou, H.C. Effect of Isomorphous Metal Substitution on the Fenton and Photo-Fenton Degradation of Methylene Blue Using Fe-Based Metal–Organic Frameworks. *ACS Appl. Mater. Interfaces* **2020**, *12*, 9292–9299. [CrossRef] [PubMed]
23. Zhao, Y.; Hou, S.; Liu, D.; Zhong, C. Effective Adsorption of Cefradine from Wastewater with a Stable Zirconium Metal–Organic Framework. *Ind. Eng. Chem. Res.* **2018**, *57*, 15132–15137. [CrossRef]
24. Zhao, X.; Zhao, H.; Dai, W.; Wei, Y.; Wang, Y.; Zhang, Y.; Zhi, L.; Huang, H.; Gao, Z. A Metal–Organic Framework with Large 1-D Channels and Rich OH Sites for High-Efficiency Chloramphenicol Removal from Water. *J. Colloid Interface Sci.* **2018**, *526*, 28–34. [CrossRef] [PubMed]
25. Huang, J.; Shan, Q.; Fang, Y.; Zhao, N.; Feng, X. Shape-Controlled Mn–Fe PBA Derived Micromotors for Organic Pollutant Removal. *New J. Chem.* **2022**, *46*, 8611–8618. [CrossRef]
26. Khan, N.A.; Najam, T.; Shah, S.S.A.; Hussain, E.; Ali, H.; Hussain, S.; Shaheen, A.; Ahmad, K.; Ashfaq, M. Development of Mn-PBA on GO Sheets for Adsorptive Removal of Ciprofloxacin from Water: Kinetics, Isothermal, Thermodynamic and Mechanistic Studies. *Mater. Chem. Phys.* **2020**, *245*, 122737. [CrossRef]
27. Yang, S.; Li, X.; Zeng, G.; Cheng, M.; Huang, D.; Liu, Y.; Zhou, C.; Xiong, W.; Yang, Y.; Wang, W.; et al. Materials Institute Lavoisier (MIL) Based Materials for Photocatalytic Applications. *Coord. Chem. Rev.* **2021**, *438*, 213874. [CrossRef]
28. Ning, R.; Pang, H.; Yan, Z.; Lu, Z.; Wang, Q.; Wu, Z.; Dai, W.; Liu, L.; Li, Z.; Fan, G.; et al. An Innovative S-Scheme AgCl/MIL-100 (Fe) Heterojunction for Visible-Light-Driven Degradation of Sulfamethazine and Mechanism Insight. *J. Hazard. Mater.* **2022**, *435*, 129061. [CrossRef]

29. Tong, J.; Chen, L.; Cao, J.; Yang, Z.; Xiong, W.; Jia, M.; Xiang, Y.; Peng, H. Biochar Supported Magnetic MIL-53-Fe Derivatives as an Efficient Catalyst for Peroxydisulfate Activation towards Antibiotics Degradation. *Sep. Purif. Technol.* **2022**, *294*, 121064. [[CrossRef](#)]
30. Xie, Y.; Liu, C.; Li, D.; Liu, Y. In Situ-Generated H<sub>2</sub>O<sub>2</sub> with NCQDs/MIL-101(Fe) by Activating O<sub>2</sub>: A Dual Effect of Photocatalysis and Photo-Fenton for Efficient Removal of Tetracycline at Natural PH. *Appl. Surf. Sci.* **2022**, *592*, 153312. [[CrossRef](#)]
31. Zhou, Q.; Liu, G. Urea-Functionalized MIL-101(Cr)@AC as a New Adsorbent to Remove Sulfacetamide in Wastewater Treatment. *Ind. Eng. Chem. Res.* **2020**, *59*, 12056–12064. [[CrossRef](#)]
32. Chen, J.; Zhang, X.; Bi, F.; Zhang, X.; Yang, Y.; Wang, Y. A Facile Synthesis for Uniform Tablet-like TiO<sub>2</sub>/C Derived from Materials of Institut Lavoisier-125(Ti) (MIL-125(Ti)) and Their Enhanced Visible Light-Driven Photodegradation of Tetracycline. *J. Colloid Interface Sci.* **2020**, *571*, 275–284. [[CrossRef](#)]
33. Hu, Q.; Dong, J.; Chen, Y.; Yi, J.; Xia, J.; Yin, S.; Li, H. In-Situ Construction of Bifunctional MIL-125(Ti)/BiOI Reactive Adsorbent/Photocatalyst with Enhanced Removal Efficiency of Organic Contaminants. *Appl. Surf. Sci.* **2022**, *583*, 152423. [[CrossRef](#)]
34. Chatterjee, A.; Jana, A.K.; Basu, J.K. A Novel Synthesis of MIL-53(Al)@SiO<sub>2</sub>: An Integrated Photocatalyst Adsorbent to Remove Bisphenol A from Wastewater. *New J. Chem.* **2020**, *44*, 18892–18905. [[CrossRef](#)]
35. Li, G.; Zhao, H.; Guo, P.; Liu, D. Effective Removal of Tinidazole by MIL-53(Al)-NDC Metal-Organic Framework from Aqueous Solution. *J. Solid State Chem.* **2022**, *310*, 123066. [[CrossRef](#)]
36. Yu, J.; Cao, J.; Yang, Z.; Xiong, W.; Xu, Z.; Song, P.; Jia, M.; Sun, S.; Zhang, Y.; Zhu, J. One-Step Synthesis of Mn-Doped MIL-53(Fe) for Synergistically Enhanced Generation of Sulfate Radicals towards Tetracycline Degradation. *J. Colloid Interface Sci.* **2020**, *580*, 470–479. [[CrossRef](#)]
37. Bergaoui, M.; Khalfaoui, M.; Awadallah-F, A.; Al-Muhtaseb, S. A Review of the Features and Applications of ZIF-8 and Its Derivatives for Separating CO<sub>2</sub> and Isomers of C<sub>3</sub>- and C<sub>4</sub>- Hydrocarbons. *J. Nat. Gas Sci. Eng.* **2021**, *96*, 104289. [[CrossRef](#)]
38. Wang, H.; Pei, X.; Kalmutzki, M.J.; Yang, J.; Yaghi, O.M. Large Cages of Zeolitic Imidazolate Frameworks. *Acc. Chem. Res.* **2022**, *55*, 707–721. [[CrossRef](#)]
39. Wang, J.; Li, Y.; Lv, Z.; Xie, Y.; Shu, J.; Alsaedi, A.; Hayat, T.; Chen, C. Exploration of the Adsorption Performance and Mechanism of Zeolitic Imidazolate Framework-8@graphene Oxide for Pb(II) and 1-Naphthylamine from Aqueous Solution. *J. Colloid Interface Sci.* **2019**, *542*, 410–420. [[CrossRef](#)]
40. Xue, W.; Zhou, Q.; Li, F.; Ondon, B.S. Zeolitic Imidazolate Framework-8 (ZIF-8) as Robust Catalyst for Oxygen Reduction Reaction in Microbial Fuel Cells. *J. Power Sources* **2019**, *423*, 9–17. [[CrossRef](#)]
41. Shafiq, S.; Al-Maythaly, B.A.; Usman, M.; Ba-Shammakh, M.S.; Al-Shammari, A.A. ZIF-95 as a Filler for Enhanced Gas Separation Performance of Polysulfone Membrane. *RSC Adv.* **2021**, *11*, 34319–34328. [[CrossRef](#)]
42. Mahmoodi, N.M.; Oveisi, M.; Bakhtiari, M.; Hayati, B.; Shekarchi, A.A.; Bagheri, A.; Rahimi, S. Environmentally Friendly Ultrasound-Assisted Synthesis of Magnetic Zeolitic Imidazolate Framework-Graphene Oxide Nanocomposites and Pollutant Removal from Water. *J. Mol. Liq.* **2019**, *282*, 115–130. [[CrossRef](#)]
43. Wang, Y.; Dai, X.; Zhan, Y.; Ding, X.; Wang, M.; Wang, X. In Situ Growth of ZIF-8 Nanoparticles on Chitosan to Form the Hybrid Nanocomposites for High-Efficiency Removal of Congo Red. *Int. J. Biol. Macromol.* **2019**, *137*, 77–86. [[CrossRef](#)] [[PubMed](#)]
44. Hu, L.; Chen, C.; Wang, X.; Hu, K.; Xu, Z. ZIF-8 Prepared in Ionic Liquid Microemulsions for Efficient Capture of Phosphate from Water. *J. Chem. Sci.* **2022**, *134*, 62. [[CrossRef](#)]
45. Miao, M.; Mu, L.; Cao, S.; Yang, Y.; Feng, X. Dual-Functional CDs@ZIF-8/Chitosan Luminescent Film Sensors for Simultaneous Detection and Adsorption of Tetracycline. *Carbohydr. Polym.* **2022**, *291*, 119587. [[CrossRef](#)]
46. Liu, S.; Ning, Y.; Qi, X.; Zhao, J.; Fu, Y.; Zhang, B.; Gao, J.; Miao, J.; Song, J.; Huo, Q. CdS-Modified ZIF-8-Derived Porous Carbon for Organic Pollutant Degradations under Visible-Light Irradiation. *Res. Chem. Intermed.* **2021**, *47*, 4193–4211. [[CrossRef](#)]
47. Fan, L.; Gong, Y.; Wan, J.; Wei, Y.; Shi, H.; Liu, C. Flower-like Molybdenum Disulfide Decorated ZIF-8-Derived Nitrogen-Doped Dodecahedral Carbon for Electro-Catalytic Degradation of Phenol. *Chemosphere* **2022**, *298*, 134315. [[CrossRef](#)]
48. Nguyen, T.B.; Thai, V.A.; Chen, C.W.; Huang, C.P.; Doong, R.; Chen, L.; Dong, C. Di N-Doping Modified Zeolitic Imidazole Framework-67 (ZIF-67) for Enhanced Peroxymonosulfate Activation to Remove Ciprofloxacin from Aqueous Solution. *Sep. Purif. Technol.* **2022**, *288*, 120719. [[CrossRef](#)]
49. Chen, G.; He, S.; Shi, G.; Ma, Y.; Ruan, C.; Jin, X.; Chen, Q.; Liu, X.; Dai, H.; Chen, X.; et al. In-Situ Immobilization of ZIF-67 on Wood Aerogel for Effective Removal of Tetracycline from Water. *Chem. Eng. J.* **2021**, *423*, 130184. [[CrossRef](#)]
50. Ren, W.; Gao, J.; Lei, C.; Xie, Y.; Cai, Y.; Ni, Q.; Yao, J. Recyclable Metal-Organic Framework/Cellulose Aerogels for Activating Peroxymonosulfate to Degrade Organic Pollutants. *Chem. Eng. J.* **2018**, *349*, 766–774. [[CrossRef](#)]
51. Li, N.; Zhou, L.; Jin, X.; Owens, G.; Chen, Z. Simultaneous Removal of Tetracycline and Oxytetracycline Antibiotics from Wastewater Using a ZIF-8 Metal Organic-Framework. *J. Hazard. Mater.* **2019**, *366*, 563–572. [[CrossRef](#)]
52. Cheng, Y.; Wang, X.; Mei, Y.; Wang, D.; Ji, C. ZnCDs/ZnO@ZIF-8 Zeolite Composites for the Photocatalytic Degradation of Tetracycline. *Catalysts* **2021**, *11*, 934. [[CrossRef](#)]
53. Wu, J.; Jin, Y.; Wu, D.; Yan, X.; Ma, N.; Dai, W. Well-Construction of Zn<sub>2</sub>SnO<sub>4</sub>/SnO<sub>2</sub>@ZIF-8 Core-Shell Hetero-Structure with Efficient Photocatalytic Activity towards Tetracycline under Restricted Space. *Chin. J. Chem. Eng.* **2022**; *in press*. [[CrossRef](#)]
54. Liu, N.; Shang, Q.; Gao, K.; Cheng, Q.; Pan, Z. Construction of ZnO/ZIF-9 Heterojunction Photocatalyst: Enhanced Photocatalytic Performance and Mechanistic Insight. *New J. Chem.* **2020**, *44*, 6384–6393. [[CrossRef](#)]

55. Ahmadi, S.A.R.; Kalaei, M.R.; Moradi, O.; Nosratinia, F.; Abdouss, M. Synthesis of Novel Zeolitic Imidazolate Framework (ZIF-67)—Zinc Oxide (ZnO) Nanocomposite (ZnO@ZIF-67) and Potential Adsorption of Pharmaceutical (Tetracycline (TCC)) from Water. *J. Mol. Struct.* **2022**, *1251*, 132013. [[CrossRef](#)]
56. Ru, J.; Wang, X.; Wang, F.; Cui, X.; Du, X.; Lu, X. UiO Series of Metal-Organic Frameworks Composites as Advanced Sorbents for the Removal of Heavy Metal Ions: Synthesis, Applications and Adsorption Mechanism. *Ecotoxicol. Environ. Saf.* **2021**, *208*, 111577. [[CrossRef](#)]
57. Yuan, N.; Gong, X.; Sun, W.; Yu, C. Chemosphere Advanced Applications of Zr-Based MOFs in the Removal of Water Pollutants. *Chemosphere* **2021**, *267*, 128863. [[CrossRef](#)]
58. Zhuang, S.; Cheng, R.; Wang, J. Adsorption of Diclofenac from Aqueous Solution Using UiO-66-Type Metal-Organic Frameworks. *Chem. Eng. J.* **2019**, *359*, 354–362. [[CrossRef](#)]
59. He, X.; Deng, F.; Shen, T.; Yang, L.; Chen, D.; Luo, J.; Luo, X.; Min, X.; Wang, F. Journal of Colloid and Interface Science Exceptional Adsorption of Arsenic by Zirconium Metal-Organic Frameworks: Engineering Exploration and Mechanism Insight. *J. Colloid Interface Sci.* **2019**, *539*, 223–234. [[CrossRef](#)]
60. Hu, D.; Song, X.; Wu, S.; Yang, X.; Zhang, H.; Chang, X.; Jia, M. Solvothermal Synthesis of Co-Substituted Phosphomolybdate Acid Encapsulated in the UiO-66 Framework for Catalytic Application in Olefin Epoxidation. *Chin. J. Catal.* **2021**, *42*, 356–366. [[CrossRef](#)]
61. Abdelmoaty, A.S.; El, S.T.; Nady, W.; Adly, F. High Performance of UiO-66 Metal—Organic Framework Modified with Melamine for Uptaking of Lead and Cadmium from Aqueous Solutions. *J. Inorg. Organomet. Polym. Mater.* **2022**, *32*, 2557–2567. [[CrossRef](#)]
62. Sena, Ş.; Selin, Ş. Acid-Modulated Zirconium Based Metal Organic Frameworks for Removal of Organic Micropollutants. *J. Environ. Chem. Eng.* **2020**, *8*, 103901. [[CrossRef](#)]
63. Yang, Q.; Wang, Y.; Wang, J.; Liu, F.; Hu, N.; Pei, H.; Yang, W.; Li, Z.; Suo, Y.; Wang, J. High Effective Adsorption/Removal of Illegal Food Dyes from Contaminated Aqueous Solution by Zr-MOFs (UiO-67). *Food Chem.* **2018**, *254*, 241–248. [[CrossRef](#)]
64. Dong, X.; Lin, Y.; Ma, Y.; Zhao, L. Ce-Doped UiO-67 Nanocrystals with Improved Adsorption Property for Removal of Organic Dyes. *RSC Adv.* **2019**, *9*, 27674–27683. [[CrossRef](#)]
65. Safaralizadeh, E.; Mahjoub, A.R.; Fazlali, F.; Bagheri, H. Facile Construction of C<sub>3</sub>N<sub>4</sub>-TE@TiO<sub>2</sub>/UiO-66 with Double Z-Scheme Structure as High Performance Photocatalyst for Degradation of Tetracycline. *Ceram. Int.* **2021**, *47*, 2374–2387. [[CrossRef](#)]
66. Zhang, X.; Zhang, N.; Gan, C.; Liu, Y.; Chen, L.; Zhang, C. Materials Science in Semiconductor Processing Synthesis of In<sub>2</sub>S<sub>3</sub>/UiO-66 Hybrid with Enhanced Photocatalytic Activity towards Methyl Orange and Tetracycline Hydrochloride Degradation under Visible-Light Irradiation. *Mater. Sci. Semicond. Process.* **2019**, *91*, 212–221. [[CrossRef](#)]
67. Sun, J.; Feng, S.; Feng, S. Hydrothermally Synthesis of MWCNT/N-TiO<sub>2</sub>/UiO-66-NH<sub>2</sub> Ternary Composite with Enhanced Photocatalytic Performance for Ketoprofen. *Inorg. Chem. Commun.* **2020**, *111*, 107669. [[CrossRef](#)]
68. Wang, Y.; Liu, C.; Wang, C.; Hu, Q.; Ding, L. 0D/3D NiCo<sub>2</sub>O<sub>4</sub>/Defected UiO-66 Catalysts for Enhanced Degradation of Tetracycline in Peroxymonosulfate/Simulated Sunlight Systems: Degradation Mechanisms and Pathways. *Chemosphere* **2022**, *299*, 134322. [[CrossRef](#)] [[PubMed](#)]
69. Uba, Z.; Ramli, A.; Jumbri, K.; Soraya, N.; Ahmad, H.; Hana, N.; Abu, H.; Saad, B. Optimization Studies and Artificial Neural Network Modeling for Pyrene Adsorption onto UiO-66 (Zr) and NH<sub>2</sub>-UiO-66 (Zr) Metal Organic Frameworks. *Polyhedron* **2020**, *192*, 114857. [[CrossRef](#)]
70. Gotthardt, M.A.; Schoch, R.; Wolf, S.; Bauer, M.; Kleist, W. Synthesis and Characterization of Bimetallic Metal–Organic Framework Cu–Ru-BTC with HKUST-1 Structure. *Dalton Trans.* **2015**, *44*, 2052–2056. [[CrossRef](#)]
71. Guo, L.; Du, J.; Li, C.; He, G.; Xiao, Y. Facile Synthesis of Hierarchical Micro-Mesoporous HKUST-1 by a Mixed-Linker Defect Strategy for Enhanced Adsorptive Removal of Benzothiophene from Fuel. *Fuel* **2021**, *300*, 120955. [[CrossRef](#)]
72. Nobar, S.N. Cu-BTC Synthesis, Characterization and Preparation for Adsorption Studies. *Mater. Chem. Phys.* **2018**, *213*, 343–351. [[CrossRef](#)]
73. Qiu, S.; Du, J.; Xiao, Y.; Zhao, Q.; He, G. Hierarchical Porous HKUST-1 Fabricated by Microwave-Assisted Synthesis with CTAB for Enhanced Adsorptive Removal of Benzothiophene from Fuel. *Sep. Purif. Technol.* **2021**, *271*, 118868. [[CrossRef](#)]
74. Forsyth, C.; Taras, T.; Johnson, A.; Zagari, J.; Collado, C.; Hoffmann, M.M.; Reed, C.R. Microwave Assisted Surfactant-Thermal Synthesis of Metal-Organic Framework Materials. *Appl. Sci.* **2020**, *10*, 4563. [[CrossRef](#)]
75. Zhang, J.; Su, C.; Xie, X.; Liu, P.; Huq, M.E. Enhanced Visible Light Photocatalytic Degradation of Dyes in Aqueous Solution Activated by HKUST-1: Performance and Mechanism. *RSC Adv.* **2020**, *10*, 37028–37034. [[CrossRef](#)]
76. Pan, J.; Bai, X.; Li, Y.; Yang, B.; Yang, P.; Yu, F.; Ma, J. HKUST-1 Derived Carbon Adsorbents for Tetracycline Removal with Excellent Adsorption Performance. *Environ. Res.* **2022**, *205*, 112425. [[CrossRef](#)]
77. Wu, Y.; Li, X.; Zhao, H.; Yao, F.; Cao, J.; Chen, Z. Core-Shell Structured Cu<sub>2</sub>O@ HKUST-1 Heterojunction Photocatalyst with Robust Stability for Highly Efficient Tetracycline Hydrochloride Degradation under Visible Light. *Chem. Eng. J.* **2021**, *426*, 131255. [[CrossRef](#)]
78. Wu, G.; Ma, J.; Li, S.; Guan, J.; Jiang, B.; Wang, L.; Li, J.; Wang, X.; Chen, L. Magnetic Copper-Based Metal Organic Framework as an Effective and Recyclable Adsorbent for Removal of Two Fluoroquinolone Antibiotics from Aqueous Solutions. *J. Colloid Interface Sci.* **2018**, *528*, 360–371. [[CrossRef](#)]
79. Yang, S.; Tang, R.; Dai, Y.; Wang, T.; Zeng, Z.; Zhang, L. Fabrication of Cellulose Acetate Membrane with Advanced Ultrafiltration Performances and Antibacterial Properties by Blending With. *Sep. Purif. Technol.* **2021**, *279*, 119524. [[CrossRef](#)]

80. Bai, K.; Fan, S.; Chen, Y.; Wang, Y.; Chen, J.; Mai, Z.; Liu, J.; Deng, L. Membrane Adsorber with Hierarchically Porous HKUST-1 Immobilized in Membrane Pores by Flowing Synthesis. *J. Membr. Sci.* **2022**, *650*, 120424. [[CrossRef](#)]
81. Seetharaj, R.; Vandana, P.V.; Arya, P.; Mathew, S. Dependence of Solvents, PH, Molar Ratio and Temperature in Tuning Metal Organic Framework Architecture. *Arab. J. Chem.* **2019**, *12*, 295–315. [[CrossRef](#)]
82. Sharanyakanth, P.S.; Radhakrishnan, M. Synthesis of Metal-Organic Frameworks (MOFs) and Its Application in Food Packaging: A Critical Review. *Trends Food Sci. Technol.* **2020**, *104*, 102–116. [[CrossRef](#)]
83. Joseph, J.; Iftexhar, S.; Srivastava, V.; Fallah, Z.; Zare, E.N.; Sillanpää, M. Iron-Based Metal-Organic Framework: Synthesis, Structure and Current Technologies for Water Reclamation with Deep Insight into Framework Integrity. *Chemosphere* **2021**, *284*, 131171. [[CrossRef](#)]
84. Rocío-Bautista, P.; Taima-Mancera, I.; Pasán, J.; Pino, V. Metal-Organic Frameworks in Green Analytical Chemistry. *Separations* **2019**, *6*, 33. [[CrossRef](#)]
85. Kumar, S.; Jain, S.; Nehra, M.; Dilbaghi, N.; Marrazza, G.; Kim, K. Green Synthesis of Metal—Organic Frameworks: A State-of-the-Art Review of Potential Environmental and Medical Applications. *Coord. Chem. Rev.* **2020**, *420*, 213407. [[CrossRef](#)]
86. Nunes, D.; Pimentel, A.; Santos, L.; Barquinha, P.; Pereira, L.; Fortunato, E.; Martins, R. Synthesis, Design, and Morphology of Metal Oxide Nanostructures. In *Metal Oxides Nanostructures*; Nunes, D., Pimentel, A., Santos, L., Pereira, L., Fortunato, E., Eds.; Elsevier: Amsterdam, The Netherlands, 2019; pp. 21–57.
87. Kashyap, A.; Singh, N.K.; Soni, M.; Soni, A. Deposition of Thin Films by Chemical Solution-Assisted Techniques. In *Chemical Solution Synthesis for Materials Design and Thin Film Device Applications*; Das, S., Dhara, S., Eds.; Elsevier: Amsterdam, The Netherlands, 2021; pp. 79–117.
88. Atikah, N.; Azuwa, M.; Nur, M.; Salehmin, I. Photocatalytic Active Metal—Organic Framework and Its Derivatives for Solar-Driven Environmental Remediation and Renewable Energy. *Coord. Chem. Rev.* **2022**, *468*, 214639. [[CrossRef](#)]
89. Ghawade, S.P.; Pande, K.N.; Dhoble, S.J.; Deshmukh, A.D. Tuning the Properties of ZnS Semiconductor by the Addition of Graphene. In *Woodhead Publishing Series in Electronic and Optical Materials*; Pawade, V.B., Dhoble, S.J., Swart, H.C., Eds.; Woodhead Publishing: Suston, UK, 2022; pp. 351–381.
90. Mohammad, N.; Abdi, J.; Oveisi, M.; Alinia, M. Metal-Organic Framework (MIL-100 (Fe)): Synthesis, Detailed Photocatalytic Dye Degradation Ability in Colored Textile Wastewater and Recycling. *Mater. Res. Bull.* **2018**, *100*, 357–366. [[CrossRef](#)]
91. Wang, Z.; Wu, C.; Zhang, Z.; Chen, Y.; Deng, W.; Chen, W. Bimetallic Fe/Co-MOFs for Tetracycline Elimination. *J. Mater. Sci.* **2021**, *56*, 15684–15697. [[CrossRef](#)]
92. Dahiya, M.S.; Tomer, V.K.; Duhan, S. Metal–Ferrite Nanocomposites for Targeted Drug Delivery. In *Woodhead Publishing Series in Biomaterials*; Inamuddin, A., Mohammad, A., Eds.; Woodhead Publishing: Suston, UK, 2018; pp. 737–760.
93. Zhang, P.; Wang, Q.; Fang, Y.; Chen, W.; Kirchon, A.A.; Baci, M.; Feng, M.; Sharma, V.K.; Zhou, H. Metal-Organic Frameworks for Capture and Degradation of Organic Pollutants. In *Metal-Organic Frameworks (MOFs) for Environmental Applications*; Ghosh, S.K., Ed.; Elsevier: Amsterdam, The Netherlands, 2019; pp. 203–229.
94. Zhao, Z.; Li, H.; Zhao, K.; Wang, L.; Gao, X. Microwave-Assisted Synthesis of MOFs: Rational Design via Numerical Simulation. *Chem. Eng. J.* **2022**, *428*, 131006. [[CrossRef](#)]
95. Kumar, A.; Kuang, Y.; Liang, Z.; Sun, X. Materials Today Nano Microwave Chemistry, Recent Advancements, and Eco-Friendly Microwave-Assisted Synthesis of Nanoarchitectures and Their Applications: A Review. *Mater. Today Nano* **2020**, *11*, 100076. [[CrossRef](#)]
96. Jiang, D.; Fang, D.; Zhou, Y.; Wang, Z.; Yang, Z.; Zhu, J. Strategies for Improving the Catalytic Activity of Metal-Organic Frameworks and Derivatives in SR-AOPs: Facing Emerging Environmental Pollutants. *Environ. Pollut.* **2022**, *306*, 119386. [[CrossRef](#)]
97. Mahmoud, M.E.; Amira, M.F.; Seleim, S.M.; Mohamed, A.K. Amino-Decorated Magnetic Metal-Organic Framework as a Potential Novel Platform for Selective Removal of Chromium (VI), Cadmium (II) and Lead (II). *J. Hazard. Mater.* **2020**, *381*, 120979. [[CrossRef](#)]
98. He, J.; Zhang, Y.; Zhang, X.; Huang, Y. Highly Efficient Fenton and Enzyme-Mimetic Activities of NH<sub>2</sub>-MIL-88B(Fe) Metal Organic Framework for Methylene Blue Degradation. *Sci. Rep.* **2018**, *8*, 5159. [[CrossRef](#)] [[PubMed](#)]
99. Arenas-Vivo, A.; Avila, D.; Horcajada, P. Phase-Selective Microwave Assisted Synthesis of Iron(III) Aminoterephthalate MOFs. *Materials* **2020**, *13*, 1469. [[CrossRef](#)] [[PubMed](#)]
100. Ren, Q.; Nie, M.; Yang, L.; Wei, F.; Ding, B.; Chen, H.; Liu, Z.; Liang, Z. Synthesis of MOFs for RhB Adsorption from Wastewater. *Inorganics* **2022**, *10*, 27. [[CrossRef](#)]
101. Chang, F.; Memon, N.; Memon, S.; Chang, A.S. Removal of Emerging Contaminants from Water by Using Fe-MOF Composite as a Sorbent. *J. Iran. Chem. Soc.* **2021**, *18*, 3249–3255. [[CrossRef](#)]
102. Ngan Tran, T.K.; Ho, H.L.; Nguyen, H.V.; Tran, B.T.; Nguyen, T.T.; Thi Bui, P.Q.; Bach, L.G. Photocatalytic Degradation of Rhodamine B in Aqueous Phase by Bimetallic Metal-Organic Framework M/Fe-MOF (M=Co, Cu, and Mg). *Open Chem.* **2022**, *20*, 52–60. [[CrossRef](#)]
103. Ploychompoo, S.; Chen, J.; Luo, H.; Liang, Q. Fast and Efficient Aqueous Arsenic Removal by Composites: Adsorption Performance and Mechanism. *J. Environ. Sci.* **2020**, *91*, 22–34. [[CrossRef](#)]
104. Xiong, P.; Zhang, H.; Li, G.; Liao, C.; Jiang, G. Adsorption Removal of Ibuprofen and Naproxen from Aqueous Solution with Cu-Doped Mil-101 (Fe). *Sci. Total Environ.* **2021**, *797*, 149179. [[CrossRef](#)]

105. Li, X.; Chen, X.; Lv, Z.; Wang, B. Ultrahigh Ciprofloxacin Accumulation and Visible-Light Photocatalytic Degradation: Contribution of Metal Organic Frameworks Carrier in Magnetic Surface Molecularly Imprinted Polymers. *J. Colloid Interface Sci.* **2022**, *616*, 872–885. [[CrossRef](#)]
106. Tabuyo-Martínez, M.; Cascos, V.; María, M.; Dur, J.; Avila-brande, D.; Prado-gonjal, J. Microwave-Assisted Synthesis of Thermoelectric Oxides and Chalcogenides. *Ceram. Int.* **2022**, *48*, 12331–12341. [[CrossRef](#)]
107. Nguyen, H.T.T.; Tran, K.N.T.; Van Tan, L.; Tran, V.A.; Doan, V.D.; Lee, T.; Nguyen, T.D. Microwave-Assisted Solvothermal Synthesis of Bimetallic Metal-Organic Framework for Efficient Photodegradation of Organic Dyes. *Mater. Chem. Phys.* **2021**, *272*, 125040. [[CrossRef](#)]
108. Abdelkareem, M.A.; Abbas, Q.; Mouselly, M.; Alawadhi, H.; Olabi, A.G. High-Performance Effective Metal–Organic Frameworks for Electrochemical Applications. *J. Sci. Adv. Mater. Devices* **2022**, *7*, 100465. [[CrossRef](#)]
109. Gascon, J. Control of Interpenetration of Copper-Based MOFs on Supported Surfaces by Electrochemical Synthesis. *CrystEngComm* **2016**, *18*, 4018–4022. [[CrossRef](#)]
110. Anumah, A.; Louis, H.; Hamzat, A.T.; Amusan, O.O. Metal-Organic Frameworks ( MOFs ): Recent Advances in Synthetic Methodologies and Some Applications. *Chem. Methodol.* **2018**, *3*, 283–305. [[CrossRef](#)]
111. Varsha, M.V.; Nageswaran, G. Review—Direct Electrochemical Synthesis of Metal Organic Frameworks Review—Direct Electrochemical Synthesis of Metal Organic Frameworks. *J. Electrochem. Soc.* **2020**, *167*, 155527. [[CrossRef](#)]
112. Ghoorchian, A.; Afkhami, A.; Madrakian, T.; Ahmadi, M. Electrochemical Synthesis of MOFs. In *Metal-Organic Frameworks for Biomedical Applications*; Mozafari, M., Ed.; Woodhead Publishing: Suston, UK, 2020; pp. 177–195.
113. Al-kutubi, H.; Gascon, J.; Sudhltter, E.J.R.; Rassaei, L. Electrosynthesis of Metal–Organic Frameworks: Challenges and Opportunities. *ChemElectroChem* **2015**, *2*, 462–474. [[CrossRef](#)]
114. Dong, Y.; Hu, T.; Pudukudy, M.; Su, H.; Jiang, L. Influence of Microwave-Assisted Synthesis on the Structural and Textural Properties of Mesoporous MIL-101 (Fe) and NH<sub>2</sub>-MIL-101 (Fe) for Enhanced Tetracycline Adsorption. *Mater. Chem. Phys.* **2020**, *251*, 123060. [[CrossRef](#)]
115. Wei, F.; Chen, D.; Liang, Z.; Zhao, S. Comparison Study on the Adsorption Capacity of Rhodamine B, Congo Red, and Orange II on Fe-MOFs. *Nanomaterials* **2018**, *8*, 248. [[CrossRef](#)]
116. Jia, Z.; Hao, S.; Wen, J.; Li, S.; Peng, W.; Huang, R.; Xu, X. Electrochemical Fabrication of Metal–Organic Frameworks Membranes and Films: A Review. *Microporous Mesoporous Mater.* **2020**, *305*, 110322. [[CrossRef](#)]
117. Campagnol, N.; Van Assche, T.; Boudewijns, T.; Denayer, J.; Binnemans, K.; De Vos, D.; Fransaeer, J. High Pressure, High Temperature Electrochemical Synthesis of Metal–Organic Frameworks: Films of MIL-100 (Fe) and HKUST-1 in Different Morphologies. *J. Mater. Chem. A* **2013**, *1*, 5827–5830. [[CrossRef](#)]
118. Wu, W.; Decker, G.E.; Weaver, A.E.; Arnoff, A.I.; Bloch, E.D.; Rosenthal, J. Facile and Rapid Room-Temperature Electrosynthesis and Controlled Surface Growth of Fe-MIL-101 and Fe-MIL-101-NH<sub>2</sub>. *ACS Cent. Sci.* **2021**, *7*, 1427–1433. [[CrossRef](#)]
119. Zhang, B.; Huang, P.; Chen, J.; Dang, X.; Hu, Y.; Ai, Y.; Zheng, D.; Chen, H. One-Step Controlled Electrodeposition of Iron-Based Binary Metal Organic Nanocomposite. *Appl. Surf. Sci.* **2020**, *504*, 144504. [[CrossRef](#)]
120. Vaitsis, C.; Sourkouni, G.; Argiris, C. Metal Organic Frameworks (MOFs) and Ultrasound: A Review. *Ultrason. Sonochem.* **2019**, *52*, 106–119. [[CrossRef](#)] [[PubMed](#)]
121. Abdollahi, N.; Yaser, M.; Morsali, A.; Junk, P.C.; Wang, J. Sonochemical Synthesis and Structural Characterization of a New Zn (II) Nanoplate Metal–Organic Framework with Removal Efficiency of Sudan Red and Congo Red. *Ultrason. Sonochem.* **2018**, *45*, 50–56. [[CrossRef](#)] [[PubMed](#)]
122. Karimi, M.; Mehrabadi, Z.; Farsadrooh, M.; Bafkary, R.; Derikvandi, H.; Hayati, P.; Mohammadi, K. Metal–Organic Framework. In *Adsorption: Fundamental Processes and Applications*; Ghaedi, M., Ed.; Elsevier: Amsterdam, The Netherlands, 2021; pp. 279–387.
123. Abdpour, S.; Kowsari, E.; Reza, M.; Moghaddam, A. Synthesis of MIL-100 (Fe)@ MIL-53 (Fe) as a Novel Hybrid Photocatalyst and Evaluation Photocatalytic and Photoelectrochemical Performance under Visible Light Irradiation. *J. Solid State Chem.* **2018**, *262*, 172–180. [[CrossRef](#)]
124. Zadeh, M.H.; Keramati, N.; Ghazi, M.M. The Effect of Solvents on Photocatalytic Activity of Fe-BTC Metal Organic Framework Obtained via Sonochemical Method. *Inorg. Nano-Metal Chem.* **2019**, *49*, 448–454. [[CrossRef](#)]
125. Taherzade, S.D.; Abbasichaleshtori, M.; Soleimannejad, J. Efficient and Ecofriendly Cellulose-Supported MIL-100(Fe) for Wastewater Treatment. *RSC Adv.* **2022**, *12*, 9023–9035. [[CrossRef](#)] [[PubMed](#)]
126. Al-attri, R.; Halladj, R.; Askari, S. Green Route of Flexible Al-MOF Synthesis with Superior Properties at Low Energy Consumption Assisted by Ultrasound Waves. *Solid State Sci.* **2022**, *123*, 106782. [[CrossRef](#)]
127. Vijayalakshmi, K.; Haq, L.N.U. Microwave-Sonochemical Synergistically Assisted Synthesis of Hybrid Ni-Fe<sub>3</sub>O<sub>4</sub>/ZnO Nanocomposite for Enhanced Antibacterial Performance. *Mater. Today Commun.* **2021**, *26*, 101835. [[CrossRef](#)]
128. Swetha, S.; Janani, B.; Khan, S.S. A Critical Review on the Development of Metal-Organic Frameworks for Boosting Photocatalysis in the Fields of Energy and Environment. *J. Clean. Prod.* **2022**, *333*, 130164. [[CrossRef](#)]
129. Sud, D.; Kaur, G. A Comprehensive Review on Synthetic Approaches for Metal-Organic Frameworks: From Traditional Solvothermal to Greener Protocols. *Polyhedron* **2021**, *193*, 114897. [[CrossRef](#)]
130. Beamish-cook, J.; Shankland, K.; Murray, C.A.; Vaqueiro, P. Insights into the Mechanochemical Synthesis of MOF-74. *Cryst. Growth Des.* **2021**, *21*, 3047–3055. [[CrossRef](#)]

131. Zhang, H.; Hu, X.; Li, T.; Zhang, Y.; Xu, H.; Sun, Y.; Gu, X.; Gu, C.; Luo, J.; Gao, B. MIL Series of Metal Organic Frameworks (MOFs) as Novel Adsorbents for Heavy Metals in Water: A Review. *J. Hazard. Mater.* **2022**, *429*, 128271. [[CrossRef](#)]
132. Chen, D.; Zhao, J.; Zhang, P.; Dai, S. Mechanochemical Synthesis of Metal–Organic Frameworks. *Polyhedron* **2019**, *162*, 59–64. [[CrossRef](#)]
133. Sylwia, G.; Szcze, B. Mechanochemistry: Toward Green Synthesis of Metal–Organic Frameworks. *Mater. Today* **2021**, *46*, 109–124. [[CrossRef](#)]
134. Pilloni, M.; Padella, F.; Ennas, G.; Lai, S.; Bellusci, M.; Rombi, E.; Sini, F.; Pentimalli, M.; Delitala, C.; Scano, A.; et al. Liquid-Assisted Mechanochemical Synthesis of an Iron Carboxylate Metal Organic Framework and Its Evaluation in Diesel Fuel Desulfurization. *Microporous Mesoporous Mater.* **2015**, *213*, 14–21. [[CrossRef](#)]
135. Jeong, H.; Lee, J. 3D-Superstructured Networks Comprising Fe-MIL-88A Metal-Organic Frameworks Under Mechanochemical Conditions. *Eur. J. Inorg. Chem.* **2019**, *42*, 4597–4600. [[CrossRef](#)]
136. He, D.; Niu, H.; He, S.; Mao, L.; Cai, Y.; Liang, Y. Strengthened Fenton Degradation of Phenol Catalyzed by Core/Shell Fe e Pd @ C Nanocomposites Derived from Mechanochemically Synthesized Fe-Metal Organic Frameworks. *Water Res.* **2019**, *162*, 151–160. [[CrossRef](#)]
137. Liu, X.; Liang, T.; Zhang, R.; Ding, Q.; Wu, S.; Li, C.; Lin, Y.; Ye, Y.; Zhong, Z.; Zhou, M. Iron-Based Metal–Organic Frameworks in Drug Delivery and Biomedicine. *ACS Appl. Mater. Interfaces* **2021**, *13*, 9643–9655. [[CrossRef](#)]
138. Ahmed, I.; Jeon, J.; Khan, N.A.; Jhung, S.H. Synthesis of a Metal–Organic Framework, Iron-Benzenetricarboxylate, from Dry Gels in the Absence of Acid and Salt. *Cryst. Growth Des.* **2012**, *12*, 5878–5881. [[CrossRef](#)]
139. Luo, Y.; Tan, B.; Liang, X.; Wang, S.; Gao, X.; Zhang, Z.; Fang, Y. Dry Gel Conversion Synthesis of Hierarchical Porous MIL-100 (Fe) and Its Water Vapor Adsorption/Desorption Performance. *Ind. Eng. Chem. Res.* **2019**, *100*, 7801–7807. [[CrossRef](#)]
140. Tannert, N.; Gökpinar, S.; Hastürk, E.; Nießing, S.; Janiak, C. Microwave-Assisted Dry-Gel Conversion—a New Sustainable Route for the Rapid Synthesis of Metal–Organic Frameworks with Solvent Re-Use. *Dalton Trans.* **2018**, *47*, 9850–9860. [[CrossRef](#)]
141. Troyano, J.; Çamur, C.; Garzón-Tovar, L.; Carné-Sánchez, A.; Imaz, I.; MasPOCH, D. Spray-Drying Synthesis of MOFs, COFs, and Related Composites. *Acc. Chem. Res.* **2020**, *53*, 1206–1217. [[CrossRef](#)]
142. Garzón-Tovar, L.; Cano-Sarabia, M.; Carné-Sánchez, A.; Carbonell, C.; Imaz, I.; MasPOCH, D. A Spray-Drying Continuous-Flow Method for Simultaneous Synthesis and Shaping of Microspherical High Nuclearity MOF Beads. *React. Chem. Eng.* **2016**, *1*, 533–539. [[CrossRef](#)]
143. Le, V.N.; Kwon, H.T.; Vo, T.K.; Kim, J.-H.; Kim, W.-S.; Kim, J. Microwave-Assisted Continuous Flow Synthesis of Mesoporous Metal-Organic Framework MIL-100 (Fe) and Its Application to Cu(I)-Loaded Adsorbent for CO/CO<sub>2</sub> Separation. *Mater. Chem. Phys.* **2020**, *253*, 123278. [[CrossRef](#)]
144. Tao, X.; Yuan, X.; Huang, L. Effects of Fe(II)/Fe(III) of Fe-MOFs on Catalytic Performance in Plasma/Fenton-like System. *Colloids Surfaces A Physicochem. Eng. Asp.* **2021**, *610*, 125745. [[CrossRef](#)]
145. Tao, X.; Sun, C.; Han, Y.; Huang, L.; Xu, D. The Plasma Assisted Preparation of Fe-MOFs with High Adsorption Capacity. *CrystEngComm* **2019**, *21*, 2541–2550. [[CrossRef](#)]
146. Tao, X.; Yuan, X.; Huang, L.; Shang, S.; Xu, D. Fe-Based Metal-Organic Frameworks as Heterogeneous Catalysts for Highly Efficient Degradation of Wastewater in Plasma/Fenton-like Systems. *RSC Adv.* **2020**, *10*, 36363–36370. [[CrossRef](#)] [[PubMed](#)]
147. Tao, X.; Cong, W.; Huang, L.; Xu, D. CeO<sub>2</sub> Photocatalysts Derived from Ce-MOFs Synthesized with DBD Plasma Method for Methyl Orange Degradation. *J. Alloys Compd.* **2019**, *805*, 1060–1070. [[CrossRef](#)]
148. Tao, X.; Sun, C.; Huang, L.; Han, Y.; Xu, D. Fe-MOFs Prepared with the DBD Plasma Method for Efficient Fenton Catalysis. *RSC Adv.* **2019**, *9*, 6379–6386. [[CrossRef](#)] [[PubMed](#)]
149. Jin, X.; Tang, T.; Tao, X.; Huang, L.; Shang, S. Regulating N Content to Anchor Fe in Fe-MOFs: Obtaining Multiple Active Sites as Efficient Photocatalysts. *J. Taiwan Inst. Chem. Eng.* **2022**, *132*, 104133. [[CrossRef](#)]
150. Miklos, D.B.; Remy, C.; Jekel, M.; Linden, K.G.; Drewes, J.E.; Hübner, U. Evaluation of Advanced Oxidation Processes for Water and Wastewater Treatment—A Critical Review. *Water Res.* **2018**, *139*, 118–131. [[CrossRef](#)]
151. Moreira, F.C.; Boaventura, R.A.R.; Brillas, E.; Vilar, V.J.P. Electrochemical Advanced Oxidation Processes: A Review on Their Application to Synthetic and Real Wastewaters. *Appl. Catal. B Environ.* **2017**, *202*, 217–261. [[CrossRef](#)]
152. Rodríguez-Narváez, O.M.; Pérez, L.S.; Yee, N.G.; Peralta-Hernández, J.M.; Bandala, E.R. Comparison between Fenton and Fenton-like Reactions for L-Proline Degradation. *Int. J. Environ. Sci. Technol.* **2019**, *16*, 1515–1526. [[CrossRef](#)]
153. Li, X.; Jie, B.; Lin, H.; Deng, Z.; Qian, J.; Yang, Y.; Zhang, X. Application of Sulfate Radicals-Based Advanced Oxidation Technology in Degradation of Trace Organic Contaminants (TrOCs): Recent Advances and Prospects. *J. Environ. Manag.* **2022**, *308*, 114664. [[CrossRef](#)]
154. Zhu, G.; Wang, S.; Yu, Z.; Zhang, L.; Wang, D.; Pang, B.; Sun, W. Application of Fe-MOFs in Advanced Oxidation Processes. *Res. Chem. Intermed.* **2019**, *45*, 3777–3793. [[CrossRef](#)]
155. Psaltou, S.; Kaprara, E.; Mitrakas, M.; Zouboulis, A. Comparative Study on Heterogeneous and Homogeneous Catalytic Ozonation Efficiency in Micropollutants’ Removal. *AQUA Water Infrastruct. Ecosyst. Soc.* **2021**, *70*, 1121–1134. [[CrossRef](#)]
156. Li, B.; Wang, Y.F.; Zhang, L.; Xu, H.Y. Enhancement Strategies for Efficient Activation of Persulfate by Heterogeneous Cobalt-Containing Catalysts: A Review. *Chemosphere* **2022**, *291*, 132954. [[CrossRef](#)]
157. Lv, H.; Zhao, H.; Cao, T.; Qian, L.; Wang, Y.; Zhao, G. Efficient Degradation of High Concentration Azo-Dye Wastewater by Heterogeneous Fenton Process with Iron-Based Metal-Organic Framework. *J. Mol. Catal. A Chem.* **2015**, *400*, 81–89. [[CrossRef](#)]

158. Liao, X.; Wang, F.; Wang, F.; Cai, Y.; Yao, Y.; Teng, B.; Hao, Q. Synthesis of (100) Surface Oriented MIL-88A-Fe with Rod-like Structure and Its Enhanced Fenton-like Performance for Phenol Removal. *Appl. Catal. B Environ.* **2019**, *259*, 118064. [[CrossRef](#)]
159. Gao, C.; Chen, S.; Quan, X.; Yu, H.; Zhang, Y. Enhanced Fenton-like Catalysis by Iron-Based Metal Organic Frameworks for Degradation of Organic Pollutants. *J. Catal.* **2017**, *356*, 125–132. [[CrossRef](#)]
160. Tang, J.; Wang, J. Fenton-like Degradation of Sulfamethoxazole Using Fe-Based Magnetic Nanoparticles Embedded into Mesoporous Carbon Hybrid as an Efficient Catalyst. *Chem. Eng. J.* **2018**, *351*, 1085–1094. [[CrossRef](#)]
161. Tang, J.; Wang, J. Iron-Copper Bimetallic Metal-Organic Frameworks for Efficient Fenton-like Degradation of Sulfamethoxazole under Mild Conditions. *Chemosphere* **2020**, *241*, 125002. [[CrossRef](#)]
162. Huang, P.; Yao, L.; Chang, Q.; Sha, Y.; Jiang, G.; Zhang, S.; Li, Z. Room-Temperature Preparation of Highly Efficient NH<sub>2</sub>-MIL-101(Fe) Catalyst: The Important Role of –NH<sub>2</sub> in Accelerating Fe(III)/Fe(II) Cycling. *Chemosphere* **2022**, *291*, 133026. [[CrossRef](#)]
163. Pu, M.; Niu, J.; Brusseau, M.L.; Sun, Y.; Zhou, C.; Deng, S. Ferrous Metal-Organic Frameworks with Strong Electron-Donating Properties for Persulfate Activation to Effectively Degrade Aqueous Sulfamethoxazole. *Chem. Eng. J.* **2020**, *394*, 125044. [[CrossRef](#)]
164. Pi, Y.; Ma, L.; Zhao, P.; Cao, Y.; Gao, H.; Wang, C.; Li, Q.; Dong, S.; Sun, J. Facile Green Synthetic Graphene-Based Co-Fe Prussian Blue Analogues as an Activator of Peroxymonosulfate for the Degradation of Levofloxacin Hydrochloride. *J. Colloid Interface Sci.* **2018**, *526*, 18–27. [[CrossRef](#)]
165. Khan, S.; Sayed, M.; Sohail, M.; Shah, L.A.; Raja, M.A. Advanced Oxidation and Reduction Processes. In *Advances in Water Purification Techniques*; Ahuja, S., Ed.; Elsevier: Amsterdam, The Netherlands, 2019; pp. 135–164.
166. Bedia, J.; Muelas-Ramos, V.; Peñas-Garzón, M.; Gómez-Avilés, A.; Rodríguez, J.J.; Belver, C. A Review on the Synthesis and Characterization of Metal Organic Frameworks for Photocatalytic Water Purification. *Catalysts* **2019**, *9*, 52. [[CrossRef](#)]
167. Llabrés i Xamena, F.X.; Corma, A.; Garcia, H. Applications for Metal–Organic Frameworks (MOFs) as Quantum Dot Semiconductors. *J. Phys. Chem. C* **2007**, *111*, 80–85. [[CrossRef](#)]
168. Boronat, M.; Climent, M.J.; Concepción, P.; Díaz, U.; García, H.; Iborra, S.; Leyva-Pérez, A.; Liu, L.; Martínez, A.; Martínez, C.; et al. A Career in Catalysis: Avelino Corma. *ACS Catal.* **2022**, *12*, 7054–7123. [[CrossRef](#)]
169. Navarathna, C.M.; Dewage, N.B.; Karunanayake, A.G.; Farmer, E.L.; Perez, F.; Hassan, E.B.; Mlsna, T.E.; Pittman, C.U. Rhodamine B Adsorptive Removal and Photocatalytic Degradation on MIL-53-Fe MOF/Magnetic Magnetite/Biochar Composites. *J. Inorg. Organomet. Polym. Mater.* **2020**, *30*, 214–229. [[CrossRef](#)]
170. Li, Y.; Xia, Y.; Liu, K.; Ye, K.; Wang, Q.; Zhang, S.; Huang, Y. Constructing Fe-MOF-Derived Z-Scheme Photocatalysts with Enhanced Charge Transport: Nanointerface and Carbon Sheath Synergistic Effect. *ACS Appl. Mater. Interfaces* **2020**, *12*, 25494–25502. [[CrossRef](#)] [[PubMed](#)]
171. Ahmad, M.; Chen, S.; Ye, F.; Quan, X.; Afzal, S.; Yu, H.; Zhao, X. Efficient Photo-Fenton Activity in Mesoporous MIL-100(Fe) Decorated with ZnO Nanosphere for Pollutants Degradation. *Appl. Catal. B Environ.* **2019**, *245*, 428–438. [[CrossRef](#)]
172. Oladipo, A.A. MIL-53 (Fe)-Based Photo-Sensitive Composite for Degradation of Organochlorinated Herbicide and Enhanced Reduction of Cr(VI). *Process Saf. Environ. Prot.* **2018**, *116*, 413–423. [[CrossRef](#)]
173. Panneri, S.; Thomas, M.; Ganguly, P.; Nair, B.N.; Mohamed, A.P.; Warriar, K.G.K.; Hareesh, U.S. C<sub>3</sub>N<sub>4</sub> Anchored ZIF 8 Composites: Photo-Regenerable, High Capacity Sorbents as Adsorptive Photocatalysts for the Effective Removal of Tetracycline from Water. *Catal. Sci. Technol.* **2017**, *7*, 2118–2128. [[CrossRef](#)]
174. Liu, X.; Zhang, J.; Dong, Y.; Li, H.; Xia, Y.; Wang, H. A Facile Approach for the Synthesis of Z-Scheme Photocatalyst ZIF-8/g-C<sub>3</sub>N<sub>4</sub> with Highly Enhanced Photocatalytic Activity under Simulated Sunlight. *New J. Chem.* **2018**, *42*, 12180–12187. [[CrossRef](#)]
175. Huang, J.; Zhang, X.; Song, H.; Chen, C.; Han, F.; Wen, C. Protonated Graphitic Carbon Nitride Coated Metal-Organic Frameworks with Enhanced Visible-Light Photocatalytic Activity for Contaminants Degradation. *Appl. Surf. Sci.* **2018**, *441*, 85–98. [[CrossRef](#)]
176. Zhang, X.; Yang, Y.; Huang, W.; Yang, Y.; Wang, Y.; He, C.; Liu, N.; Wu, M.; Tang, L. G-C<sub>3</sub>N<sub>4</sub>/UiO-66 Nanohybrids with Enhanced Photocatalytic Activities for the Oxidation of Dye under Visible Light Irradiation. *Mater. Res. Bull.* **2018**, *99*, 349–358. [[CrossRef](#)]
177. Giannakoudakis, D.A.; Travlou, N.A.; Secor, J.; Bandosz, T.J. Oxidized G-C<sub>3</sub>N<sub>4</sub> Nanospheres as Catalytically Photoactive Linkers in MOF/g-C<sub>3</sub>N<sub>4</sub> Composite of Hierarchical Pore Structure. *Small* **2017**, *13*, 1601758. [[CrossRef](#)]
178. Shi, L.; Wang, T.; Zhang, H.; Chang, K.; Ye, J. Electrostatic Self-Assembly of Nanosized Carbon Nitride Nanosheet onto a Zirconium Metal–Organic Framework for Enhanced Photocatalytic CO<sub>2</sub> Reduction. *Adv. Funct. Mater.* **2015**, *25*, 5360–5367. [[CrossRef](#)]
179. Pan, Y.; Hu, X.; Bao, M.; Li, F.; Li, Y.; Lu, J. Fabrication of MIL-Fe (53)/Modified g-C<sub>3</sub>N<sub>4</sub> Photocatalyst Synergy H<sub>2</sub>O<sub>2</sub> for Degradation of Tetracycline. *Sep. Purif. Technol.* **2021**, *279*, 119661. [[CrossRef](#)]
180. Jun, Y.-S.; Lee, E.Z.; Wang, X.; Hong, W.H.; Stucky, G.D.; Thomas, A. From Melamine-Cyanuric Acid Supramolecular Aggregates to Carbon Nitride Hollow Spheres. *Adv. Funct. Mater.* **2013**, *23*, 3661–3667. [[CrossRef](#)]
181. Guo, R.; Nengzi, L.-C.; Chen, Y.; Song, Q.; Gou, J.; Cheng, X. Construction of High-Efficient Visible Photoelectrocatalytic System for Carbamazepine Degradation: Kinetics, Degradation Pathway and Mechanism. *Chin. Chem. Lett.* **2020**, *31*, 2661–2667. [[CrossRef](#)]
182. Dowd, K.O.; Pillai, S.C. Photo-Fenton Disinfection at near Neutral PH: Process, Parameter Optimization and Recent Advances. *J. Environ. Chem. Eng.* **2020**, *8*, 104063. [[CrossRef](#)]
183. Ameta, R.; Chohadia, A.K.; Jain, A.; Punjabi, P.B. Fenton and Photo-Fenton Processes. In *Advanced Oxidation Processes for Waste Water Treatment*; Ameta, S.C., Ameta, R., Eds.; Academic Press: Cambridge, MA, USA, 2018; pp. 49–87.

184. Liu, B.; Wu, Y.; Han, X.; Lv, J.; Zhang, J.; Shi, H. Facile Synthesis of G-C<sub>3</sub>N<sub>4</sub>/Amine-Functionalized MIL-101(Fe) Composites with Efficient Photocatalytic Activities under Visible Light Irradiation. *J. Mater. Sci. Mater. Electron.* **2018**, *29*, 17591–17601. [[CrossRef](#)]
185. Li, Y.; Fang, Y.; Cao, Z.; Li, N.; Chen, D.; Xu, Q.; Lu, J. Construction of G-C<sub>3</sub>N<sub>4</sub>/PDI@MOF Heterojunctions for the Highly Efficient Visible Light-Driven Degradation of Pharmaceutical and Phenolic Micropollutants. *Appl. Catal. B Environ.* **2019**, *250*, 150–162. [[CrossRef](#)]
186. Li, X.; Pi, Y.; Wu, L.; Xia, Q.; Wu, J.; Li, Z.; Xiao, J. Facilitation of the Visible Light-Induced Fenton-like Excitation of H<sub>2</sub>O<sub>2</sub> via Heterojunction of g-C<sub>3</sub>N<sub>4</sub>/NH<sub>2</sub>-Iron Terephthalate Metal-Organic Framework for MB Degradation. *Appl. Catal. B Environ.* **2017**, *202*, 653–663. [[CrossRef](#)]
187. Wang, J.S.; Yi, X.H.; Xu, X.; Ji, H.; Alanazi, A.M.; Wang, C.C.; Zhao, C.; Kaneti, Y.V.; Wang, P.; Liu, W.; et al. Eliminating Tetracycline Antibiotics Matrix via Photoactivated Sulfate Radical-Based Advanced Oxidation Process over the Immobilized MIL-88A: Batch and Continuous Experiments. *Chem. Eng. J.* **2022**, *431*, 133213. [[CrossRef](#)]
188. Yi, X.; Ji, H.; Wang, C.; Li, Y.; Li, Y.; Zhao, C.; Wang, A.; Fu, H.; Wang, P.; Zhao, X.; et al. Photocatalysis-Activated SR-AOP over PDINH/MIL-88A (Fe) Composites for Boosted Chloroquine Phosphate Degradation: Performance, Mechanism, Pathway and DFT Calculations. *Appl. Catal. B Environ.* **2021**, *293*, 120229. [[CrossRef](#)]
189. Lin, Y.; Zhang, Y.; Li, G. Promotion of Sulfameter Degradation by Coupling Persulfate and Photocatalytic Advanced Oxidation Processes with Fe-Doped MOFs. *Sep. Purif. Technol.* **2022**, *282*, 119632. [[CrossRef](#)]
190. Ruan, Y.; Kong, L.; Zhong, Y.; Diao, Z.; Shih, K.; Wang, S.; Chen, D. Review on the Synthesis and Activity of Iron-Based Catalyst in Catalytic Oxidation of Refractory Organic Pollutants in Wastewater. *J. Clean. Prod.* **2021**, *321*, 128924. [[CrossRef](#)]
191. He, Z.; Liu, Y.; Wang, J.; Lv, Y.; Xu, Y.; Jia, S. Enhanced Degradation of Old Landfill Leachate in Heterogeneous Electro-Fenton Catalyzed Using Fe<sub>3</sub>O<sub>4</sub> Nano-Particles Encapsulated by Metal Organic Frameworks. *J. Clean. Prod.* **2021**, *321*, 128947. [[CrossRef](#)]
192. Wang, Y.; Zhao, M.; Hou, C.; Chen, W.; Li, S.; Ren, R.; Li, Z. Efficient Degradation of Perfluorooctanoic Acid by Solar Photo-Electro-Fenton like System Fabricated by MOFs/Carbon Nanofibers Composite Membrane. *Chem. Eng. J.* **2021**, *414*, 128940. [[CrossRef](#)]
193. Ren, G.; Zhou, M.; Liu, M.; Ma, L.; Yang, H. A Novel Vertical-Flow Electro-Fenton Reactor for Organic Wastewater Treatment. *Chem. Eng. J.* **2016**, *298*, 55–67. [[CrossRef](#)]
194. Lu, J.-Y.; Yuan, Y.-R.; Hu, X.; Liu, W.-J.; Li, C.-X.; Liu, H.-Q.; Li, W.-W. MOF-Derived Fe<sub>2</sub>O<sub>3</sub>/Nitrogen/Carbon Composite as a Stable Heterogeneous Electro-Fenton Catalyst. *Ind. Eng. Chem. Res.* **2020**, *59*, 1800–1808. [[CrossRef](#)]
195. Ye, Z.; Schukraft, G.E.M.; L'Hermitte, A.; Xiong, Y.; Brillas, E.; Petit, C.; Sirés, I. Mechanism and Stability of an Fe-Based 2D MOF during the Photoelectro-Fenton Treatment of Organic Micropollutants under UVA and Visible Light Irradiation. *Water Res.* **2020**, *184*, 115986. [[CrossRef](#)]
196. Du, X.; Fu, W.; Su, P.; Cai, J.; Zhou, M. Internal-Micro-Electrolysis-Enhanced Heterogeneous Electro-Fenton Process Catalyzed by Fe/Fe<sub>3</sub>C@PC Core-Shell Hybrid for Sulfamethazine Degradation. *Chem. Eng. J.* **2020**, *398*, 125681. [[CrossRef](#)]
197. Le, T.X.H.; Cowan, M.G.; Drobek, M.; Bechelany, M.; Julbe, A.; Cretin, M. Fe-Nanoporous Carbon Derived from MIL-53(Fe): A Heterogeneous Catalyst for Mineralization of Organic Pollutants. *Nanomaterials* **2019**, *9*, 641. [[CrossRef](#)]
198. Tang, J.; Wang, J. MOF-Derived Three-Dimensional Flower-like FeCu@C Composite as an Efficient Fenton-like Catalyst for Sulfamethazine Degradation. *Chem. Eng. J.* **2019**, *375*, 122007. [[CrossRef](#)]
199. Du, X.; Fu, W.; Su, P.; Zhang, Q.; Zhou, M. S-doped MIL-53 as efficient heterogeneous electro-Fenton catalyst for degradation of sulfamethazine at circumneutral pH. *J. Hazard. Mater.* **2022**, *424*, 127674. [[CrossRef](#)]
200. Liu, K.; Yu, M.; Wang, H.; Wang, J.; Liu, W. Multiphase Porous Electrochemical Catalysts Derived from Iron- Based Metal – Organic Framework Compounds. *Environ. Sci. Technol.* **2019**, *53*, 6474–6482. [[CrossRef](#)]
201. Fu, A.; Liu, Z.; Sun, Z. Cu/Fe Oxide Integrated on Graphite Felt for Degradation of Sulfamethoxazole in the Heterogeneous Electro-Fenton Process under near-Neutral Conditions. *Chemosphere* **2022**, *297*, 134257. [[CrossRef](#)]
202. Ye, Z.; Padilla, J.A.; Xuriguera, E.; Beltran, J.L.; Alcaide, F.; Brillas, E.; Sirés, I. A Highly Stable Metal-Organic Framework-Engineered FeS<sub>2</sub>/C Nanocatalyst for Heterogeneous Electro-Fenton Treatment: Validation in Wastewater at Mild PH. *Environ. Sci. Technol.* **2020**, *54*, 4664–4674. [[CrossRef](#)] [[PubMed](#)]
203. Ye, Z.; Padilla, J.A.; Xuriguera, E.; Brillas, E.; Sirés, I. Magnetic MIL(Fe)-Type MOF-Derived N-Doped Nano-ZVI@C Rods as Heterogeneous Catalyst for the Electro-Fenton Degradation of Gemfibrozil in a Complex Aqueous Matrix. *Appl. Catal. B Environ.* **2020**, *266*, 118604. [[CrossRef](#)]
204. Du, X.; Fu, W.; Su, P.; Zhang, Q.; Zhou, M. FeMo@porous Carbon Derived from MIL-53(Fe)@MoO<sub>3</sub> as Excellent Heterogeneous Electro-Fenton Catalyst: Co-Catalysis of Mo. *J. Environ. Sci.* **2023**, *127*, 652–666. [[CrossRef](#)]
205. Qi, C.; Han, S.; Lin, J.; Cheng, J.; Du, K.; Hu, Y.; Chen, Y. Reconstruction of Electronic Structure of MOF-525 via Metalloporphyrin for Enhanced Photoelectro-Fenton Process. *Catalysts* **2022**, *12*, 671. [[CrossRef](#)]
206. Du, X.; Su, P.; Fu, W.; Zhang, Q.; Zhou, M. Heterogeneous Photoelectro-Fenton Catalyzed by FeCu@PC for Efficient Degradation of Sulfamethazine. *Electrochim. Acta* **2022**, *412*, 140122. [[CrossRef](#)]
207. Hang, J.; Yi, X.-H.; Wang, C.-C.; Fu, H.; Wang, P.; Zhao, Y. Heterogeneous Photo-Fenton Degradation toward Sulfonamide Matrix over Magnetic Fe<sub>3</sub>S<sub>4</sub> Derived from MIL-100(Fe). *J. Hazard. Mater.* **2022**, *424*, 127415. [[CrossRef](#)]
208. Chavoshani, A.; Hashemi, M.; Amin, M.M.; Ameta, S.C. Pharmaceuticals as Emerging Micropollutants in Aquatic Environments. In *Micropollutants and Challenges*; Ameta, S.C., Chavoshani, A., Hashemi, M., Amin, M.M., Eds.; Academic Press: London, UK, 2020; pp. 35–90.

209. Martín-Pozo, L.; Gómez-Regalado, M.d.C.; García-Córcoles, M.T.; Zafra-Gómez, A. Removal of Quinolone Antibiotics from Wastewaters and Sewage Sludge. In *Emerging Contaminants in the Environment*; Sarma, H., Dominguez, D.C., Lee, W.-Y., Eds.; Elsevier: Amsterdam, The Netherlands, 2022; pp. 381–406.
210. Rekhate, C.V.; Srivastava, J.K. Recent Advances in Ozone-Based Advanced Oxidation Processes for Treatment of Wastewater—A Review. *Chem. Eng. J. Adv.* **2020**, *3*, 100031. [[CrossRef](#)]
211. Linden, K.G.; Mohseni, M. Advanced Oxidation Processes: Applications in Drinking Water Treatment. In *Comprehensive Water Quality and Purification*; Ahuja, S., Ed.; Elsevier: Waltham, MA, USA, 2014; pp. 148–172.
212. Ikehata, K.; Li, Y. Ozone-Based Processes. In *Emerging Green Chemical Technology*; Ameta, S.C., Ameta, R., Eds.; Academic Press: London, UK, 2018; pp. 115–134. [[CrossRef](#)]
213. Mohebbi, H.; Moussavi, G.; Karimi, M.; Giannakis, S. Catalytic Ozonation of Acetaminophen with a Magnetic, Cerium-Based Metal-Organic Framework as a Novel, Easily-Separable Nanocomposite. *Chem. Eng. J.* **2022**, *434*, 134614. [[CrossRef](#)]
214. Chen, H.; Wang, J. MOF-Derived  $\text{Co}_3\text{O}_4\text{-C@FeOOH}$  as an Efficient Catalyst for Catalytic Ozonation of Norfloxacin. *J. Hazard. Mater.* **2021**, *403*, 123697. [[CrossRef](#)]
215. Yu, D.; Li, L.; Wu, M.; Crittenden, J.C. Enhanced Photocatalytic Ozonation of Organic Pollutants Using an Iron- Based Metal-Organic Framework. *Appl. Catal. B Environ.* **2019**, *251*, 66–75. [[CrossRef](#)]
216. Pattappan, D.; Kavya, K.V.; Vargheese, S.; Kumar, R.T.R.; Haldorai, Y. Graphitic Carbon Nitride/NH<sub>2</sub>-MIL-101(Fe) Composite for Environmental Remediation: Visible-Light-Assisted Photocatalytic Degradation of Acetaminophen and Reduction of Hexavalent Chromium. *Chemosphere* **2022**, *286*, 131875. [[CrossRef](#)]
217. Huang, W.; Liu, W.; Yang, Z.; Chen, Y.; Li, G.; Liao, X. MIL-88A Anchoring on Different Morphological g-C<sub>3</sub>N<sub>4</sub> for Enhanced Fenton Performance. *Microporous Mesoporous Mater.* **2022**, *329*, 111531. [[CrossRef](#)]
218. Yu, R.; Ma, R.; Wang, L.; Bai, L.; Yang, S.; Qian, J. Activation of Peroxydisulfate (PDS) by Bi<sub>5</sub>O<sub>7</sub>I@MIL-100 (Fe) for Catalytic Degradation of Aqueous Doxycycline (DOX) under UV Light Irradiation: Characteristic, Performance and Mechanism. *J. Water Process Eng.* **2022**, *48*, 102903. [[CrossRef](#)]
219. Tang, L.; Lv, Z.; Xue, Y.; Xu, L.; Qiu, W.; Zheng, C. MIL-53 (Fe) Incorporated in the Lamellar BiOBr: Promoting the Visible-Light Catalytic Capability on the Degradation of Rhodamine B and Carbamazepine. *Chem. Eng. J.* **2019**, *374*, 975–982. [[CrossRef](#)]
220. Liu, N.; Wang, J.; Wu, J.; Li, Z.; Huang, W.; Zheng, Y.; Lei, J.; Zhang, X.; Tang, L. Magnetic Fe<sub>3</sub>O<sub>4</sub>@MIL-53(Fe) Nanocomposites Derived from MIL-53(Fe) for the Photocatalytic Degradation of Ibuprofen under Visible Light Irradiation. *Mater. Res. Bull.* **2020**, *132*, 111000. [[CrossRef](#)]
221. He, L.; Dong, Y.; Zheng, Y.; Jia, Q.; Shan, S.; Zhang, Y. A Novel Magnetic MIL-101(Fe)/TiO<sub>2</sub> Composite for Photo Degradation of Tetracycline under Solar Light. *J. Hazard. Mater.* **2019**, *361*, 85–94. [[CrossRef](#)]
222. Fakhri, H.; Farzadkia, M.; Boukherroub, R.; Srivastava, V.; Sillanpää, M. Design and Preparation of Core-Shell Structured Magnetic Graphene Oxide@MIL-101(Fe): Photocatalysis under Shell to Remove Diazinon and Atrazine Pesticides. *Sol. Energy* **2020**, *208*, 990–1000. [[CrossRef](#)]
223. Zhong, Z.; Li, M.; Fu, J.; Wang, Y.; Muhammad, Y.; Li, S. Construction of Cu-Bridged Cu<sub>2</sub>O/MIL (Fe/Cu) Catalyst with Enhanced Interfacial Contact for the Synergistic Photo-Fenton Degradation of Thiacloprid. *Chem. Eng. J.* **2020**, *395*, 125184. [[CrossRef](#)]
224. Liang, H.; Liu, R.; An, X.; Hu, C.; Zhang, X.; Liu, H. Bimetal-Organic Frameworks with Coordinatively Unsaturated Metal Sites for Highly Efficient Fenton-like Catalysis. *Chem. Eng. J.* **2021**, *414*, 128669. [[CrossRef](#)]
225. Fdez-Sanromán, A.; Pazos, M.; Sanroman, A. Peroxymonosulphate Activation by Basolite F-300 for *Escherichia coli* Disinfection and Antipyrine Degradation. *Int. J. Environ. Res. Public Health* **2022**, *19*, 6852. [[CrossRef](#)]
226. He, W.; Li, Z.; Lv, S.; Niu, M.; Zhou, W.; Li, J.; Lu, R.; Gao, H.; Pan, C.; Zhang, S. Facile Synthesis of Fe<sub>3</sub>O<sub>4</sub>@MIL-100(Fe) towards Enhancing Photo-Fenton like Degradation of Levofloxacin via a Synergistic Effect between Fe<sub>3</sub>O<sub>4</sub> and MIL-100(Fe). *Chem. Eng. J.* **2021**, *409*, 128274. [[CrossRef](#)]
227. Yang, T.; Yu, D.; Wang, D.; Yang, T.; Li, Z.; Wu, M.; Petru, M.; Crittenden, J. Accelerating Fe(III)/Fe(II) Cycle via Fe(II) Substitution for Enhancing Fenton-like Performance of Fe-MOFs. *Appl. Catal. B Environ.* **2021**, *286*, 119859. [[CrossRef](#)]
228. Yang, W.; Hong, P.; Yang, D.; Yang, Y.; Wu, Z.; Xie, C.; He, J.; Zhang, K.; Kong, L.; Liu, J. Enhanced Fenton-like Degradation of Sulfadiazine by Single Atom Iron Materials Fixed on Nitrogen-Doped Porous Carbon. *J. Colloid Interface Sci.* **2021**, *597*, 56–65. [[CrossRef](#)]
229. Ping, C.; Yi, C.; Wei, Z.; Yu, S.; Yan, X.; Zhi, C.; Fang, Y.; Jun, S. Facile Synthesis of Porphyrin-MOFs with High Photo-Fenton Activity to Efficiently Degrade Ciprofloxacin. *J. Colloid Interface Sci.* **2022**, *622*, 690–699. [[CrossRef](#)]
230. Tian, H.; Peng, J.; Du, Q.; Hui, X.; He, H. One-Pot Sustainable Synthesis of Magnetic MIL-100(Fe) with Novel Fe<sub>3</sub>O<sub>4</sub> Morphology and Its Application in Heterogeneous Degradation. *Dalton Trans.* **2018**, *47*, 3417–3424. [[CrossRef](#)]
231. Zhao, Q.; Wang, C.; Wang, P. Effective Norfloxacin Elimination via Photo-Fenton Process over the MIL-101(Fe)-NH<sub>2</sub> Immobilized on  $\alpha\text{-Al}_2\text{O}_3$  Shee. *Chin. Chem. Lett.* **2022**, *33*, 4828–4833. [[CrossRef](#)]
232. Zhang, Z.; Chen, X.; Tan, Y.; Jiang, C.; Wang, H.; Zhang, S. Preparation of Millimeter-Scale MIL-53 (Fe)@ Polyethersulfone Balls to Optimize Photo-Fenton Process. *Chem. Eng. J.* **2022**, *441*, 135881. [[CrossRef](#)]
233. Liu, N.; Zheng, Y.; Jing, C.; Gao, B.; Huang, W.; Li, Z.; Lei, J.; Zhang, X.; Cui, L.; Tang, L. Boosting Catalytic Degradation Efficiency by Incorporation of MIL-53 (Fe) with Ti<sub>3</sub>C<sub>2</sub>T<sub>x</sub> Nanosheets. *J. Mol. Liq.* **2020**, *311*, 113201. [[CrossRef](#)]
234. Tan, C.; Lu, X.; Cui, X.; Jian, X.; Hu, Z.; Dong, Y.; Liu, X.; Huang, J.; Deng, L. Novel Activation of Peroxymonosulfate by an Easily Recyclable VC@Fe<sub>3</sub>O<sub>4</sub> Nanoparticles for Enhanced Degradation of Sulfadiazine. *Chem. Eng. J.* **2019**, *363*, 318–328. [[CrossRef](#)]

- 
235. Zhou, X.; Xu, D.; Chen, Y.; Hu, Y. Enhanced Degradation of Triclosan in Heterogeneous E-Fenton Process with MOF-Derived Hierarchical Mn/Fe@PC Modified Cathode. *Chem. Eng. J.* **2020**, *384*, 123324. [[CrossRef](#)]
236. Liu, M.; Feng, Z.; Luan, X.; Chu, W.; Zhao, H.; Zhao, G. Accelerated Fe<sup>2+</sup> Regeneration in an Effective Electro-Fenton Process by Boosting Internal Electron Transfer to a Nitrogen-Conjugated Fe(III) Complex. *Environ. Sci. Technol.* **2021**, *55*, 6042–6051. [[CrossRef](#)] [[PubMed](#)]